

# Topological Vibration Analysis of Elastic Lattices via Bloch Sphere Mapping

Kazi T. Mahmood and M. Arif Hasan\*

Department of Mechanical Engineering, Wayne State University, Detroit, MI 48202

kazi.mahmood@wayne.edu, hasan.arif@wayne.edu

## Abstract

Mechanical lattices support topological wave phenomena governed by geometric phases. We develop a compact Hilbert space description for one-dimensional elastic chains, expressing intra-cell motion as a normalized superposition of orthogonal eigenstates and tracking complex amplitudes as trajectories on a Bloch sphere. For diatomic lattices, this construction makes inversion symmetry protection explicit: the relative phase between in-phase and out-of-phase modes is piecewise locked, and the Zak phase is quantized with band-dependent jumps at symmetry points. Extending the framework to triatomic lattices shows that restoring inversion retains quantization, whereas breaking it dequantizes the geometric phase while leaving the spectrum origin invariant. Viewing norm-preserving transformations of the modal coefficient pair as Bloch-sphere rotations, we demonstrate classical analogues of single-qubit logic gates: a  $\pi$ -phase rotation about a transverse axis swaps the modal poles, and a longitudinal-axis phase flip maps balanced superpositions to their conjugates. These gate-like operations are realized by controlled evolution across wavenumber space and can be driven or reprogrammed through spatiotemporal stiffness modulation. Introducing space-time modulation hybridizes carrier and sideband harmonics, producing continuous phase winding and open-path geometric phases accumulated along the Floquet trajectory. Across static and modulated regimes, the framework unifies algebraic and geometric viewpoints, is robust to gauge and basis choices, and operates directly on amplitude-phase data. Results clarify how symmetry, modulation, and topology jointly govern dispersion, modal mixing, and phase accumulation, providing tools to analyze and design vibration and acoustic functionalities in engineered structures.

## 1 Introduction

Topological mechanics has revealed that mechanical lattices—assemblies of masses and springs obeying Newton’s laws—can emulate the robust wave phenomena long associated with electronic, photonic, and atomic systems [1, 2]. A central organizing idea is the geometric phase accumulated by eigenstates as a control parameter (e.g., the Bloch wavenumber) is varied. In crystalline solids, the one-dimensional (1D) Berry—or Zak—phase is quantized (to 0 or  $\pi$ ) by inversion symmetry and encodes bulk information with interfacial consequences, establishing an early bridge between band topology and material response [3, 4]. Within classical and quantum wave systems alike, the geometric phase extends beyond the original adiabatic, cyclic setting: Samuel and Bhandari showed that neither cyclic evolution nor unitarity is required, enabling the definition of open-path phases determined by the Pancharatnam connection between nonorthogonal states [5]. These ideas have catalyzed a broader program in topological phononics and mechanics, where symmetry-protected transport, boundary localization, and defect-bound modes have been designed and observed in architected structures [6, 7].

In this context, elastic mass-spring chains serve a transparent platform to investigate how symmetry, dispersion, and modulation collaborate to create nontrivial topology. For 1D bands, inversion symmetry constrains the Zak phase to 0 or  $\pi$ , making it a sensitive diagnostic of how a unit cell is arranged and where its origin is chosen [3, 8]. Recent work has also clarified that time-dependent, space-time modulated lattices break reciprocity and hybridize carrier harmonics with Floquet sidebands, enriching dispersion and enabling direction-dependent gaps

---

\*Corresponding author: hasan.arif@wayne.edu

[9]. Together, these developments lead to a description that treats state geometry—amplitudes and phases—as primary entities, together with the eigenfrequencies themselves.

Our earlier studies introduced the Spectral Analysis of Amplitudes and Phases (SAAP) method, which uses molecular-dynamics (MD) simulations under tailored initial conditions to extract complex modal amplitudes, phases, and associated Berry (Zak) phases in periodic elastic superlattices [10, 11]. SAAP revealed how inversion-symmetric unit cells enforce Berry-phase quantization, and how varying spring arrangements or changing the unit-cell origin toggles between 0 and  $\pi$  without affecting the spectrum. Operationally, SAAP first determines the band structure  $\omega_j(k)$  and then, in a second MD pass with traveling-wave initial conditions, projects the displacement field onto plane waves to obtain band-indexed complex amplitudes  $a_n^j(k)$ ; a normalized amplitude vector per band is then used to compute a discrete Berry connection and the Zak phase. Consequently, SAAP yields geometric phases and amplitude profiles indexed by band over the Brillouin zone but does not provide compact, gauge-robust state-coefficient trajectories that expose how a single lattice state navigates an internal basis across  $k$  or time; it also presumes periodicity and closed paths in wavenumber  $k$ , making open-path phases and space–time modulation cumbersome to treat. The present manuscript addresses these limitations directly. We recast intra-cell motion as a normalized superposition of orthogonal eigenstates and use the resulting complex coefficients as intrinsic coordinates for the state on a Bloch sphere. In this representation, phases and amplitude hierarchies become geometry; Berry/Zak phases appear as windings of state trajectories; and the effects of symmetry and modulation are read off from paths on  $S^2$ . Thus, our approach differs from common eigenvector-inner-product routes. Rather than inferring Berry/Zak phases indirectly, we construct the state coefficients directly and map their evolution to the Bloch sphere. This “algebraic (coefficients)–geometric (sphere trajectories) unification” makes symmetry-enforced plateaus, jumps, and windings in phases geometrically transparent and provides a gauge-invariant way to treat static and time-modulated lattices within a single language. By moving beyond band-level phase extraction to explicit, gauge-robust state-coefficient trajectories on the Bloch sphere, we provide a compact, symmetry-aware, and experimentally tractable framework that links intra-cell state geometry to Berry/Zak and open-path phases in both static and space–time-modulated elastic chains.

The remainder of the paper is organized as follows. Section 2 defines the mass–spring lattice, boundary conditions, and unit-cell choices underpinning the analysis. Section 3 develops the Bloch-sphere formulation for time-independent lattices, highlighting inversion-symmetry-protected quantization in diatomic cells and its controlled breakdown in triatomic cells. Section 4 extends the framework to space–time modulated lattices, demonstrating open-path geometric phases and modulation-induced windings consistent with Floquet hybridization. Section 5 concludes by situating the contributions relative to the broader literature on space–time modulation and topological mechanics.

## 2 Elastic Lattice Under Consideration

The objective of this study is to represent the eigenstates that carry Berry phases as classical superpositions of normal modes in a one-dimensional elastic lattice. The lattice comprises identical point masses connected by linear (harmonic) springs in a periodic chain. Each lattice contains  $N_c$  unit cells; each unit cell contains  $N_m$  masses. We impose Born-von Kármán boundary conditions so that  $e^{ikLN_c} = 1$ , where  $L$  is the unit-cell length and  $k$  is the Bloch wave number. Consequently, the first Brillouin zone is discretized as  $k \in [-\pi, \pi)$  with spacing  $2\pi/N_c$ . The Brillouin zone is the reciprocal-space domain of unique wave vectors that encode the periodic wave dynamics.

Two prototypical cells are analyzed in detail: Diatomic cell ( $N_m = 2$ )—the minimal configuration that admits acoustic and optical bands. Triatomic cell ( $N_m = 3$ )—the simplest system in which Berry-phase quantization can be lifted when inversion symmetry is broken. Throughout, we treat time-independent and, later in the manuscript, time-dependent stiffness modulations; the former builds the foundation for the superposition formalism and its geometric interpretation on the Bloch sphere, while the latter extends the approach beyond strict periodicity. The latter case extends the accessible Hilbert-space trajectories from a great-circle arc to the full Bloch sphere, thereby demonstrating a classical analogue of qubit control.

### 3 Lattice with Time-Independent Stiffness

#### 3.1 Diatomic Unit Cell

We consider a diatomic unit cell composed of identical masses coupled by nearest-neighbor springs of stiffness  $\psi_1$  and  $\psi_2$ , arranged periodically and subject to Born-von Kármán boundary conditions. Our aim is twofold: (i) to obtain closed-form acoustic/optical traveling-wave solutions and their complex amplitudes, and (ii) to recast the lattice motion as a normalized superposition of two orthogonal eigenstates, thereby exposing how inversion symmetry fixes the relative phase (0 or  $\pi$ ) across the Brillouin zone—the 1D Zak-phase quantization that we later visualize on a Bloch sphere. The quantization of the Zak phase in inversion-symmetric 1D lattices and its origin dependence are well established and provide the topological backdrop for our superposition analysis [3].

##### 3.1.1 Traveling-Wave Ansatz and Dispersion

Let  $u_1(t)$  and  $u_2(t)$  denote the displacements of the two masses within a given unit cell  $N_i$ . The linear equations of motion are

$$\begin{aligned} m\ddot{u}_{1,N_i}(t) &= \psi_2 [u_{2,N_{i-1}}(t) - u_{1,N_i}(t)] - \psi_1 [u_{1,N_i}(t) - u_{2,N_i}(t)], \\ m\ddot{u}_{2,N_i}(t) &= \psi_1 [u_{1,N_i}(t) - u_{2,N_i}(t)] - \psi_2 [u_{2,N_i}(t) - u_{1,N_{i+1}}(t)] \end{aligned} \quad (1)$$

We seek Bloch traveling-wave solutions with the compact ansatz (periodic in reciprocal space).

$$u_{1,N_i}(t) = A_1 e^{i(kN_i L + \omega t)}, \quad u_{2,N_i}(t) = A_2 e^{i(kN_i L + \omega t)}. \quad (2)$$

Substitution of (2) into (1) yields the dispersion relation and the band-dependent complex amplitude ratio. In particular, the amplitudes satisfy,

$$\frac{A_1}{A_2} = \pm \frac{\sqrt{\tau}}{\sqrt{\tau^*}}, \quad \tau = \psi_1 + \psi_2 e^{-ikL} \quad (3)$$

and the acoustic/optical branch selection can be expressed compactly as [10]:

$$\begin{aligned} \text{Acoustic branch:} \quad & \begin{pmatrix} A_1 \\ A_2 \end{pmatrix} = \begin{pmatrix} \sqrt{\tau} \\ \sqrt{\tau^*} \end{pmatrix}, \\ \text{Optical branch:} \quad & \begin{pmatrix} A_1 \\ A_2 \end{pmatrix} = \begin{pmatrix} \sqrt{e^{-i\pi}\tau} \\ \sqrt{e^{+i\pi}\tau^*} \end{pmatrix}. \end{aligned}$$

Together with the familiar acoustic (+) and optical (−) branches dispersion relation:

$$\omega_{\pm}^2 = \frac{\psi_1 + \psi_2}{m} \left[ 1 \pm \sqrt{1 - \frac{4\psi_1\psi_2}{(\psi_1 + \psi_2)^2} \sin^2 \frac{kL}{2}} \right].$$

These are the standard diatomic chain results cast in the compact ansatz; they are unitarily equivalent to those obtained with a general ansatz and therefore will yield identical Berry connections and Berry phases, consistent with prior analyses of ansatz invariance [10].

##### 3.1.2 Superposition Basis and Bloch-Sphere Representation

Because the dynamics are linear, the two independent eigenstates within a unit cell may be chosen orthonormally as an in-phase mode  $E_1 = \frac{1}{\sqrt{2}} \begin{pmatrix} 1 \\ 1 \end{pmatrix}$  and an out-of-phase mode  $E_2 = \frac{1}{\sqrt{2}} \begin{pmatrix} 1 \\ -1 \end{pmatrix}$  (a convenient "pseudospin" basis). The cell-wise displacement vector can then be written as a normalized superposition,

$$\vec{U} \equiv \begin{bmatrix} u_1 \\ u_2 \end{bmatrix} = \begin{bmatrix} A_1 \\ A_2 \end{bmatrix} e^{i(kN_i L + \omega t)} \equiv (\alpha E_1 + \beta E_2) e^{i\omega t} \quad (4)$$

with complex coefficients  $\alpha, \beta$ . Using (3)–(4) and the relation  $A_2 = A_1^*$ , one convenient normalization leads to

$$\begin{aligned}\hat{\alpha} &= \frac{1}{|\operatorname{Re}(A_1)| + |\operatorname{Im}(A_1^*)|} \frac{1}{\sqrt{2}} (A_1 + A_1^*) e^{ikN_i L}, \\ \hat{\beta} &= \frac{1}{|\operatorname{Re}(A_1)| + |\operatorname{Im}(A_1^*)|} \frac{1}{\sqrt{2}} (A_1 - A_1^*) e^{ikN_i L}.\end{aligned}\tag{5}$$

so that

$$\arg(\hat{\alpha}) - \arg(\hat{\beta}) = \arg\left[\frac{1}{\sqrt{2}}(A_1 + A_1^*)e^{ikN_i L}\right] - \arg\left[\frac{1}{\sqrt{2}}(A_1 - A_1^*)e^{ikN_i L}\right].$$

Because  $A_1 + A_1^*$  is real,  $\arg[\frac{1}{\sqrt{2}}(A_1 + A_1^*)e^{ikN_i L}] = kN_i L + \arg(\mathbb{R}(A_1 + A_1^*))$ ; depending on the notation of the  $\mathbb{R}(A_1 + A_1^*)$ , the argument of the term is either 0 ( $\mathbb{R}(A_1 + A_1^*) > 0$ ) or  $\pi$  ( $\mathbb{R}(A_1 + A_1^*) < 0$ ); And because  $A_1 - A_1^*$  is purely imaginary,  $\arg[\frac{1}{\sqrt{2}}(A_1 - A_1^*)e^{ikN_i L}] = -\frac{\pi}{2} \operatorname{sgn}(\operatorname{Im}(A_1 - A_1^*)) + kN_i L$ .

Two consequences are immediate and central to this manuscript. First, inversion symmetry enforces a quantized relative phase between  $\hat{\alpha}$  and  $\hat{\beta}$ : across the Brillouin zone the argument difference is restricted to 0 or  $\pi$ , mirroring the quantized Zak phase in 1D inversion-symmetric lattices. Second, the assignment of  $\arg(\hat{\alpha}) - \arg(\hat{\beta})$  to 0 or  $\pi$  is branch-dependent: on the acoustic branch, the phases follow the  $k$ -parities encoded by (4), with  $\arg(\hat{\alpha}) - \arg(\hat{\beta}) = 0$  for  $k < 0$  and  $\pi$  for  $k > 0$ , while the optical branch exhibits the complementary behavior. These selection rules rationalize the observed  $0/\pi$  Berry phases for  $\psi_1 \geq \psi_2$  and are consistent with earlier predictions and with the invariance of Berry quantities under unitary changes of ansatz and origin [10]. Finally, interpreting  $(\alpha, \beta)$  as a classical two-level state will provide a direct geometric mapping to the Bloch sphere familiar from two-mode wave physics; this mapping will be used below to visualize band-resolved state trajectories and to contrast our superposition framework with earlier works [3, 12, 13].

The superposition-based formulation above is parallel to quantum two-level kinematics but remains entirely classical; it provides state-vector geometry— $(\hat{\alpha}, \hat{\beta})$  on a Bloch sphere—that is directly tied to inversion symmetry and Berry/Zak phase quantization, while remaining unitarily equivalent (in Berry quantities) to general-ansatz treatments used in prior work. The present framework will later accommodate broken periodicity and time-dependent stiffness without sacrificing a clear geometric interpretation. This conceptual bridge is what distinguishes the present manuscript from earlier analyses: it demonstrates classical superpositions in elastic lattices that are isomorphic to qubit superpositions and uses the Bloch sphere to represent—and reason about—their topological phases [14, 15].

### 3.1.3 Acoustic and Optical Branches: Explicit Coefficient Forms

The explicit expressions for the superposition coefficients  $\alpha$  and  $\beta$  on the acoustic and optical branches provide a real-space view of how inversion symmetry constrains the relative phase of the two basis states.

#### Acoustic Branch

For the first unit cell, the normalized superposition coefficients  $(\hat{\alpha}, \hat{\beta})$  that weight the in-phase and out-of-phase basis states are written in terms of the complex scalar  $\tau$  as

$$\begin{pmatrix} \hat{\alpha} \\ \hat{\beta} \end{pmatrix} = \frac{1}{|\operatorname{Re} \tau| + |\operatorname{Im} \tau|} \frac{1}{\sqrt{2}} e^{ikL} \begin{pmatrix} \tau + \tau^* \\ \tau - \tau^* \end{pmatrix}.\tag{6}$$

In the following discussion, we introduce the stiffness-ordering parameter.

$$\Delta \equiv \psi_1 - \psi_2$$

so that  $\Delta > 0$  corresponds to  $\psi_1 > \psi_2$  and  $\Delta < 0$  to  $\psi_1 < \psi_2$ . Define also the small offset from the Brillouin-zone (BZ) edge  $kL = \pm\pi$  by  $kL = \mp\pi + \varepsilon$  with  $\varepsilon \rightarrow 0^\pm$ .

Using the explicit form of  $\tau$  from the two-mass solution and expanding at the BZ edges, one finds the following limiting expressions. First, for

$$kL = -\pi + \varepsilon, \quad \varepsilon \rightarrow 0,$$

the coefficient vector reduces to

$$\begin{pmatrix} \hat{\alpha} \\ \hat{\beta} \end{pmatrix} = \frac{1}{\operatorname{Re}(\Delta e^{-i\varepsilon}) + \operatorname{Im}(\Delta e^{-i\varepsilon})} \left[ -\frac{1}{\sqrt{2}} \begin{pmatrix} 2e^{i\varepsilon} \operatorname{Re}(\Delta e^{-i\varepsilon}) \\ \operatorname{Re}(\Delta e^{-i\varepsilon}) - \operatorname{Re}(\Delta e^{+i\varepsilon}) \end{pmatrix} \right]$$

since  $(1 + e^{-i(-\pi+\varepsilon)}) \approx 0$ . Taking  $\varepsilon \rightarrow 0$  gives two cases:

**Case I** ( $\Delta > 0$ , i.e.,  $\psi_1 > \psi_2$ ):

$$\begin{pmatrix} \hat{\alpha} \\ \hat{\beta} \end{pmatrix} = \begin{pmatrix} -1 \\ 0 \end{pmatrix}.$$

**Case II** ( $\Delta < 0$ , write  $\Delta = -\delta$  with  $\delta > 0$ , i.e.,  $\psi_1 < \psi_2$ ):

$$\begin{pmatrix} \hat{\alpha} \\ \hat{\beta} \end{pmatrix} = \begin{pmatrix} 0 \\ -i \end{pmatrix}.$$

Similarly, for

$$kL = \pi - \varepsilon, \quad \varepsilon \rightarrow 0,$$

one obtains

$$\begin{pmatrix} \hat{\alpha} \\ \hat{\beta} \end{pmatrix} = \frac{1}{\operatorname{Re}(\Delta e^{+i\varepsilon}) + \operatorname{Im}(\Delta e^{+i\varepsilon})} \left[ -\frac{1}{\sqrt{2}} \begin{pmatrix} 2e^{-i\varepsilon} \operatorname{Re}(\Delta e^{-i\varepsilon}) \\ \operatorname{Re}(\Delta e^{-i\varepsilon}) - \operatorname{Re}(\Delta e^{+i\varepsilon}) \end{pmatrix} \right]$$

again because  $(1 + e^{-i(-\pi+\varepsilon)}) \approx 0$ . Taking the limit  $\varepsilon \rightarrow 0$ :

**Case I** ( $\Delta > 0, \psi_1 > \psi_2$ ):

$$\begin{pmatrix} \hat{\alpha} \\ \hat{\beta} \end{pmatrix} = \begin{pmatrix} -1 \\ 0 \end{pmatrix}.$$

**Case II** ( $\Delta < 0, \Delta = -\delta < 0$ ):

$$\begin{pmatrix} \hat{\alpha} \\ \hat{\beta} \end{pmatrix} = \begin{pmatrix} 0 \\ i \end{pmatrix},$$

which differs from  $\begin{pmatrix} 0 \\ -i \end{pmatrix}$  by a global  $\pi$  phase, i.e., a physically irrelevant gauge choice for the spinor.

On the acoustic branch, the phase of the ratio  $\hat{\alpha}/\hat{\beta}$  is pinned to 0 or  $\pi$  on each side of the BZ, and flips upon crossing  $k = 0$ . Crucially, the sign of  $k$  (not the ordering of  $\psi_1, \psi_2$ ) selects which of the two real relative phases is realized—this is the real-space manifestation of the inversion-protected, quantized Zak phase in 1D. In other words, the acoustic-branch spinor toggles between two diametrically opposite longitudes on the Bloch sphere as  $k$  traverses the zone. This is exactly the  $0/\pi$  pattern expected for inversion-symmetric lattices (SSH-type physics) [16, 17, 8]

## Optical Branch

An analogous calculation applies to the optical branch, for which the expression reads

$$\begin{pmatrix} \hat{\alpha} \\ \hat{\beta} \end{pmatrix} = \frac{1}{|\operatorname{Re}(\sqrt{e^{-i\pi\tau}})| + |\operatorname{Im}(\sqrt{e^{-i\pi\tau}})|} \frac{1}{\sqrt{2}} e^{ikL} \begin{pmatrix} \sqrt{e^{-i\pi\tau}} + \sqrt{e^{-i\pi\tau^*}} \\ \sqrt{e^{-i\pi\tau}} - \sqrt{e^{-i\pi\tau^*}} \end{pmatrix}. \quad (7)$$

Evaluating the same edge limits:

For  $kL = -\pi + \varepsilon, \varepsilon \rightarrow 0$ ,

$$\begin{pmatrix} \hat{\alpha} \\ \hat{\beta} \end{pmatrix} = \frac{-1}{|\operatorname{Re}(\sqrt{\Delta e^{-i(\pi+\varepsilon)}})| + |\operatorname{Im}(\sqrt{\Delta e^{-i(\pi+\varepsilon)}})|} \frac{1}{\sqrt{2}} e^{i\varepsilon} \begin{pmatrix} \sqrt{\Delta e^{-i(\pi+\varepsilon)}} + \sqrt{\Delta e^{+i(\pi+\varepsilon)}} \\ \sqrt{\Delta e^{-i(\pi+\varepsilon)}} - \sqrt{\Delta e^{+i(\pi+\varepsilon)}} \end{pmatrix}.$$

**Case 1** ( $\Delta > 0, \psi_1 > \psi_2$ ):

$$\begin{pmatrix} \hat{\alpha} \\ \hat{\beta} \end{pmatrix} = \begin{pmatrix} -i \\ 0 \end{pmatrix}.$$

**Case 2** ( $\Delta < 0$ , put  $\Delta = -\delta, \delta > 0$ , i.e.,  $\psi_1 < \psi_2$ ):

$$\begin{pmatrix} \hat{\alpha} \\ \hat{\beta} \end{pmatrix} = \begin{pmatrix} -1 \\ 0 \end{pmatrix}.$$

For  $kL = \pi - \varepsilon, \varepsilon \rightarrow 0$ , the same algebra yields:

**Case 1** ( $\Delta > 0$ ):

$$\begin{pmatrix} \hat{\alpha} \\ \hat{\beta} \end{pmatrix} = \begin{pmatrix} -i \\ 0 \end{pmatrix}.$$

**Case 2** ( $\Delta < 0$ ):

$$\begin{pmatrix} \hat{\alpha} \\ \hat{\beta} \end{pmatrix} = \begin{pmatrix} -1 \\ 0 \end{pmatrix}.$$

Collecting the four edge limits for the acoustic and optical branches shows that the relative phase between the two coefficients is constant (either 0 or  $\pi/2$  modulo  $\pi$ ) on a given side of the BZ and flips only when crossing  $kL = 0$ . Equivalently, we will show that the spinor  $(\alpha, \beta)$  (or  $(\hat{\alpha}, \hat{\beta})$ ) will lie on a fixed great-circle arc of the Bloch sphere on each side and undergoes a discrete azimuthal jump at the zone center. This is the canonical signature of inversion-protected  $0/\pi$  Zak phases in one dimension: on choosing the unit-cell origin, one exchanges the two quantized values, and the piecewise-constant relative phase reflects that gauge freedom [16, 18].

In contrast with earlier works [19], the explicit coefficient forms above make the classical two-state superposition structure completely transparent: each band eigenstate is a normalized spinor  $\hat{\alpha}|E_1\rangle + \hat{\beta}|E_2\rangle$  whose trajectory on the Bloch sphere will encode the Berry/Zak phase accrued as  $k$  winds the BZ. That geometric viewpoint—classically realized here—has been the standard language for qubits and two-level systems and will underpin our Bloch-sphere visualizations and Berry-phase computations in the rest of the paper.

In inversion-symmetric 1D lattices (such as the diatomic chain studied here), the Zak phase of an isolated band is quantized to 0 or  $\pi$ ; the two possibilities are exchanged by moving the unit-cell origin, and the phase jump occurs at the BZ symmetry point—precisely the behavior recovered by the limiting forms above. This connects our classical superpositions directly to the SSH-family topological invariant and to contemporary measurements/derivations of Zak phases in 1D photonic/acoustic analogs [8, 16, 20].

While previous studies derive Berry/Zak phases from amplitude-vector overlaps, the explicit closed-form spinors at the BZ edges (Eqs. (6)–(7) and the four limits) let us read off the relative phase locking and the ensuing Zak class directly, and then will map those states (see Sec. 3.2) onto a Bloch sphere to visualize classical superpositions that mirror qubit states. This dual algebraic-geometric representation—classical superposition coefficients and two-state Bloch sphere—clarifies how stiffness ordering and the sign of  $k$  select the longitude on sphere, offering a compact, physically transparent route to the same topological conclusions and providing a platform for extending the analysis (Sec. 4) to time-modulated lattices via non-cyclic geometric phases [17].

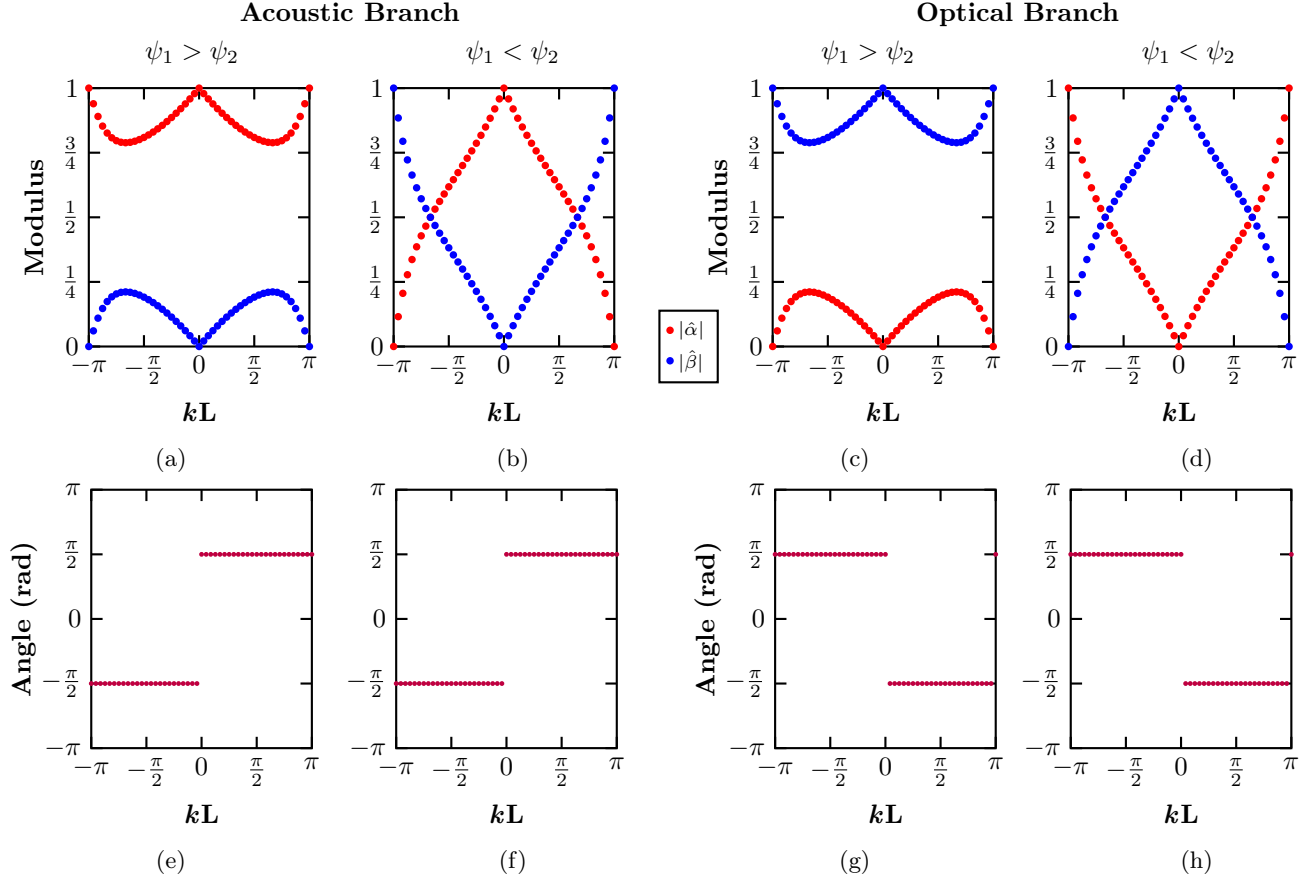


Figure 1: **Top Panel:** Modulus of complex amplitudes  $|\hat{\alpha}|$  and  $|\hat{\beta}|$  of two mutually orthogonal states  $|E_1\rangle$  and  $|E_2\rangle$ . **Bottom Panel:** phase difference between the amplitude moduli.

Figure 1 shows the normalized superposition coefficients of Eq. (5) across the first Brillouin zone  $kL \in [-\pi, \pi]$ . Panel (a) and (b) shows the moduli  $|\hat{\alpha}|$  and  $|\hat{\beta}|$  that weight the two mutually orthogonal eigenstates  $|E_1\rangle$  and  $|E_2\rangle$ . For the illustrative stiffness ordering  $(\psi_1, \psi_2) = (1, 1/2)$ —and, more generally, whenever  $\psi_1 > \psi_2$ —the acoustic branch is dominated by the  $|E_1\rangle$  component, i.e.,  $|\hat{\alpha}| > |\hat{\beta}|$ ; the situation inverts on the optical branch, for which  $|\hat{\beta}|$  dominates (Fig. 1c). Except at the high-symmetry points  $kL = -\pi, 0, \pi$ , both  $|\hat{\alpha}|$  and  $|\hat{\beta}|$  remain appreciable over substantial portions of the zone, indicating a mixed superposition rather than a pure-state selection. And, for the stiffness ordering  $(\psi_1, \psi_2) = (2, 1)$ , which means,  $\psi_1 < \psi_2$ , the acoustic branch is dominated by the  $|E_2\rangle$  component, i.e.,  $|\hat{\alpha}| < |\hat{\beta}|$  (Fig. 1b). Similar to before case, this phenomena flips at the optical branch (Fig. 1d).

From Figs. 1e and 1f, we see that the relative phase  $\Delta\phi = \arg(\hat{\alpha}) - \arg(\hat{\beta})$  locks to  $-\pi/2$  or  $+\pi/2$  and switches between those values when  $kL$  advances by  $\pi$  (i.e., upon crossing the zone midpoint). Consequently,  $\Delta\phi$  is piecewise constant with a jump of  $\pi$  at the inversion-symmetric point. However, the individual absolute phases evolve smoothly with  $kL \in [-\pi, \pi]$ . For the case  $\psi_1 > \psi_2$  (Fig. 1e), the phase of  $\beta$  acquires two twists of  $\pi$  after one closed traversal of the Brillouin zone, whereas the phase of  $\hat{\alpha}$  changes monotonically without such a twist. This phenomena inverts on the optical branch (Fig. 1g). On the contrary, for the case  $\psi_1 < \psi_2$  (Fig. 1f and 1h), both the phases of  $\hat{\alpha}$  and  $\hat{\beta}$  acquire a single twist of  $\pi$  after one closed traversal of the Brillouin zone for the acoustic and optical branch. This behavior is consistent with the in-phase/out-of-phase character of acoustic/optical modes in diatomic chains and with inversion-symmetry-protected quantization of the Zak (Berry) phase to 0 or  $\pi$  in one-dimensional lattices [3].

With the coefficients  $(\hat{\alpha}, \hat{\beta})$  in hand, the state of the diatomic unit cell can be mapped to a point on the Bloch sphere by defining polar ( $\theta$ ) and azimuthal ( $\varphi$ ) angles in terms of  $\hat{\alpha}$  and  $\hat{\beta}$ . In our two-mass problem, the in-phase ( $E_1$ ) and out-of-phase ( $E_2$ ) eigenstates play the role of the north and south poles, respectively, and the superposed lattice state traces a longitude as  $kL$  traverses the Brillouin zone. Thus, the inversion-protected  $\{0, \pi\}$  Zak phases correspond geometrically to whether the closed path on the sphere carries an odd or even

number of twists; Sec. 3.3 visualizes this correspondence and computes the Berry connection explicitly. This two-level geometric description follows the standard qubit parameterization and provides a compact lens for reading phase locking and  $|\hat{\alpha}|/|\hat{\beta}|$  dominance directly from trajectories on  $S^2$  [16].

The branch selection, amplitude symmetry, and Berry-phase conclusions summarized above agree with both general 1D topological-band theory and our previous SAAP studies of periodic chains. In particular, for the two-mass cell we indeed find a Berry phase of 0 when  $\psi_1 > \psi_2$  and  $\pi$  when  $\psi_1 < \psi_2$  (modulo the choice of origin), matching analytical solutions as well as MD/SAAP computations reported previously. What is distinctive here is the classical-superposition framework—we demonstrate that the elastic state itself can be written and manipulated as  $\hat{\alpha}|E_1\rangle + \hat{\beta}|E_2\rangle$ , and that its evolution over  $k$  traces well-defined loops whose winding encodes the Zak phase. This geometric-dynamical picture complements the standard bulk-invariant statements (e.g., Zak phase in inversion-symmetric 1D systems) and clarifies how the same binary topology manifests in measurable amplitude-phase data—precisely the bridge our procedure was designed to provide. Moreover, by tying the locked  $\Delta\phi = \pm\pi/2$  plateaus and the  $|\hat{\alpha}|/|\hat{\beta}|$  hierarchy to the paths on  $S^2$ , the manuscript makes contact with contemporary measurements of the Zak phase in classical and quantum platforms and with its role in predicting interface states in inversion-symmetric 1D media [21, 22].

Quantized Berry/Zak phases in 1D inversion-symmetric lattices are a bedrock result of topological band theory; casting the diatomic chain as a two-level classical superposition makes that structure explicit and portable. The same machinery we use here generalizes to the symmetry-broken and time-modulated lattices treated later in the manuscript, where it helps distinguish non-quantized geometric phases from origin-convention effects and connects phase winding to mode hybridization. In this way the work advances prior treatments by showing that classical elastic states can realize quantum-style superpositions while reproducing the expected  $\{0, \pi\}$  Zak classes—and by doing so it directly outputs the complex coefficients needed to compute Berry connections and phases [23].

## 3.2 Geometric Representation on the Bloch Sphere and Evaluation of the Zak (Berry) Phase

Having extracted the complex, normalized modal coefficients for the diatomic unit cell, we can treat the lattice as an analogous two-level (qubit-like) system. This perspective allows us to visualize the continuous mixing of the in-phase ( $|E_1\rangle$ ) and out-of-phase ( $|E_2\rangle$ ) eigenvectors as a trajectory on the surface of the Bloch sphere  $S^2$ ; and to compute the associated geometric (Zak) phase directly from that trajectory, without appealing to auxiliary gauge choices. Both steps are carried out below and culminate in an explicit, classical analogue of the quantum-mechanical Bloch-sphere formalism—one of the salient contributions of the present work.

### 3.2.1 Bloch-Sphere Parameterization

Following the standard two-component spinor notation, we write

$$\hat{\alpha} = \cos\left(\frac{\theta}{2}\right), \quad \hat{\beta} = e^{i\varphi} \sin\left(\frac{\theta}{2}\right) \quad (8)$$

so that the polar angle  $\theta \in [0, \pi]$  encodes the relative weight of the two eigenstates while the azimuth  $\varphi \in [-\pi, \pi]$  stores their relative phase. The north pole ( $\theta = 0$ ) therefore represents the pure in-phase state  $|E_1\rangle$ , the south pole ( $\theta = \pi$ ) its out-of-phase companion  $|E_2\rangle$ , and any point on the sphere corresponds to a coherent, classical superposition

$$|\psi(k)\rangle = \hat{\alpha}(k)|E_1\rangle + \hat{\beta}(k)|E_2\rangle \equiv \cos\left(\frac{\theta(k)}{2}\right)|E_1\rangle + e^{i\varphi(k)} \sin\left(\frac{\theta(k)}{2}\right)|E_2\rangle.$$

To anchor the geometry, we evaluate  $(\theta, \varphi)$  for three  $k$ -points (overall normalization is omitted for brevity):

Near a band extremum. For the state sampled at  $kL = -1.57$ , the amplitudes lead to

$$\begin{pmatrix} \hat{\alpha} \\ \hat{\beta} \end{pmatrix} = \begin{pmatrix} -0.0006 - 0.0001i \\ -0.9497 - 0.3111i \end{pmatrix} = (0.0006e^{-i\pi})|E_1\rangle + (0.9994e^{-i\pi})|E_2\rangle = \cos\frac{\theta}{2}|E_1\rangle + e^{i\varphi} \sin\frac{\theta}{2}|E_2\rangle,$$

with the angles identified as  $\theta = \pi$  and  $\varphi = 0$ . Geometrically the state sits at the south pole (pure  $E_2$ ), as expected when one mode dominates.

Near the opposite extremum. For  $kL = 0.0654$ , we obtain

$$\begin{aligned} \begin{pmatrix} \hat{\alpha} \\ \hat{\beta} \end{pmatrix} &= \begin{pmatrix} -0.9857 - 0.1680i \\ -8.6397 \times 10^{-5} - 1.9891 \times 10^{-5}i \end{pmatrix} = (0.9999e^{-i\pi}) |E_1\rangle + (8.8657 \times 10^{-5} e^{-i\pi}) |E_2\rangle \\ &= \cos \frac{\theta}{2} |E_1\rangle + e^{i\varphi} \sin \frac{\theta}{2} |E_2\rangle \end{aligned}$$

with  $\theta = 0$  and  $\varphi = 0$ . The state is at the north pole (pure  $E_1$ ).

Nonseparable superposition At  $kL = -0.4254$ , the amplitudes yield

$$\begin{pmatrix} \hat{\alpha} \\ \hat{\beta} \end{pmatrix} = \begin{pmatrix} -0.5888 - 0.0386i \\ 0.0266 - 0.4091i \end{pmatrix} = (0.5091e^{-i\pi}) |E_1\rangle + (0.4099e^{-i\frac{\pi}{2}}) |E_2\rangle = \cos \frac{\theta}{2} |E_1\rangle + e^{i\varphi} \sin \frac{\theta}{2} |E_2\rangle,$$

with  $\theta = \frac{\pi}{2}$  and  $\varphi = \frac{\pi}{2}$ . This corresponds to a balanced, classically nonseparable (i.e., phase-coherent) superposition with the state proportional to  $(|E_1\rangle + i|E_2\rangle)$  up to overall normalization. The geometry is now on the equator at azimuth  $\varphi = \pi/2$ .

These points confirm that the lattice state moves smoothly between the poles and the equator as  $k$  sweeps the Brillouin zone, exactly mirroring the interchange of the modulus hierarchy  $|\hat{\alpha}| \gtrless |\hat{\beta}|$  identified in Fig. 1. Using Eq. (8) at every discretized  $k$ , we reconstruct the full path  $[\theta(k), \varphi(k)]$  on the sphere (Fig. 2).

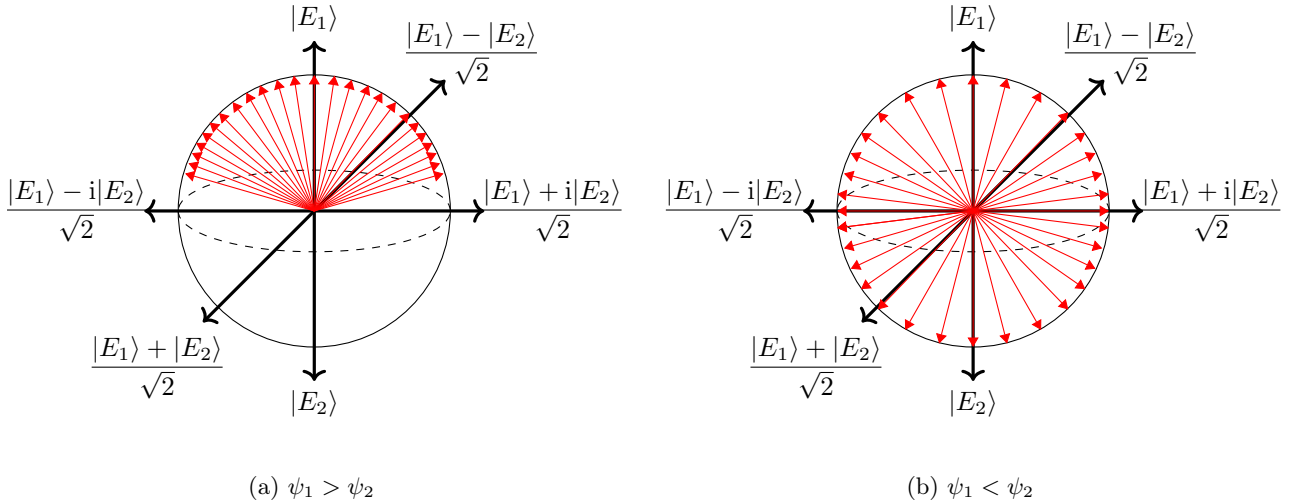


Figure 2: Bloch state demonstration of change of state between  $|E_1\rangle$  and  $|E_2\rangle$  at a two-mass system depicted in Hilbert Space with different stiffness matrices for the two cases (a)  $\psi_1 > \psi_2$  (b)  $\psi_1 < \psi_2$  at the acoustic branch.

From Fig. 1a ( $\psi_1 > \psi_2$ ) we have seen that the modulus hierarchy  $|\hat{\alpha}| > |\hat{\beta}|$  holds over broad  $k$ -intervals, hence from Fig. 2a it is clear that the trajectory hugs the  $|E_1\rangle$  pole: the system repeatedly approaches the pure state  $|E_1\rangle$  whenever the real part of the masses dominates.  $\hat{\alpha}$  dominance yields a state geometrically aligned with  $|E_1\rangle$  because domination here refers to the modulus associated with the in-phase eigenvector. The corresponding polar angle remains in the "polar cap,"  $\theta \in (-\pi/2, +\pi/2)$ , i.e., the path does not cross the equator except near isolated  $k$  where  $|\hat{\alpha}| \approx |\hat{\beta}|$ . In contrast, Fig. 2b ( $\psi_1 < \psi_2$ ) does not bias the dynamics toward either  $|E_1\rangle$  or  $|E_2\rangle$ : the trajectory makes a full longitude-like revolution ( $\theta$  runs from  $-\pi$  to  $+\pi$ ) without ever settling at a perfectly pure  $|E_1\rangle$  or  $|E_2\rangle$  state (the path skirts the pole but does not terminate there).

In both stiffness orderings, the azimuth  $\varphi$  is confined to a  $\pi$ -wide window,  $\varphi \in [-\pi/2, +\pi/2]$ , as dictated by the measured phase difference  $\Delta\varphi = \arg(\hat{\alpha}) - \arg(\hat{\beta})$ . This constraint is visible in Figs. 1e–f: as  $k$  passes through the zone center, the relative phase undergoes a discrete jump of magnitude  $\pi$ , sending  $\Delta\varphi$  from  $-\pi/2$  to  $+\pi/2$  (or vice versa). That sign flip of the relative phase—equivalently, a reversal of the spinor's azimuth—encodes the usual  $0/\pi$  Zak-phase bifurcation in inversion-symmetric 1D lattices [24].

Putting the two stiffness orderings side-by-side clarifies the accessible regions on  $S^2$ . For  $\psi_1 < \psi_2$  the trajectory explores a much larger fraction of the sphere: starting near  $|E_2\rangle$ , varying  $k$  drives the state through equatorial mixtures  $(|E_1\rangle + i|E_2\rangle)/\sqrt{2}$  and then toward  $|E_1\rangle$  before a  $\pi$  jump returns it to the opposite hemisphere;

subsequent evolution repeats the pattern until the loop closes back near  $|E_2\rangle$ . For  $\psi_1 > \psi_2$  the loop is more localized: it begins at (or near)  $|E_1\rangle$  and oscillates around the equator between  $(|E_1\rangle - i|E_2\rangle)/\sqrt{2}$  without ever approaching the  $|E_2\rangle$  pole. In short,  $\psi_1 < \psi_2$  enables a broader sweep of superposed states within the same  $k$ -span, whereas  $\psi_1 > \psi_2$  confines the dynamics to a single longitude family. The contrast highlights a central result of this paper: changing the spring-constant hierarchy toggles the accessible portion of the Bloch sphere and hence the class of elastic superpositions that can be realized. This tunability is the classical parallel to manipulating a quantum bit on its Bloch sphere. By linking a macroscopic design knob (the spring-stiffness ratio) to the solid angle swept on  $S^2$ , we provide an intuitive handle for engineering topological phase transitions in mechanical lattices.

### 3.2.2 Quantum Analogue Logic Gates

Having mapped the diatomic lattice to a two-level Hilbert space spanned by  $(|E_1\rangle, |E_2\rangle)$ , we represent the normalized state vector  $(\hat{\alpha}, \hat{\beta})$  as a point on the Bloch sphere. In this representation, any norm-preserving transformation of  $(\hat{\alpha}, \hat{\beta})$  corresponds to a rotation on the sphere, exactly as in a single-qubit system. Accordingly, logic gates in the present mechanical setting are realized as unitary maps that rotate the classical superposition state on  $S^2$ . We point out that while the physical system is entirely classical, the kinematics of these transformations is isomorphic to the  $SU(2)$  action on the Bloch sphere familiar from quantum information. This relates how band-resolved states evolve across the Brillouin zone and under space-time modulation, and to connect those evolution to gate-like operations.

Throughout, we adopt the computational basis  $|E_1\rangle, |E_2\rangle$ . Because phases and global signs depend on the ansatz and band labeling (Sec. 3.1), matrix representatives of elementary gates may differ by overall phases or sign conventions from conventional quantum logic gates; what matters physically is the induced rotation on the sphere and the relative phase between components, which are basis-invariant. This is also exploited in quantum mechanics, where different but unitarily equivalent conventions generate identical Bloch-sphere trajectories and Berry/Zak phases.

**Pauli-(Y)-type inversion about the (y)-axis.** At  $kL = -\pi$ , the complex amplitude coefficients take the form  $\begin{pmatrix} 0 \\ -i \end{pmatrix}$  which corresponds to the south-pole state  $|E_2\rangle$ . Acting with the (conventionally phased)  $y$ -axis inversion,

$$\begin{bmatrix} 0 & i \\ -i & 0 \end{bmatrix} \begin{pmatrix} 0 \\ -i \end{pmatrix} = \begin{pmatrix} 1 \\ 0 \end{pmatrix}$$

advances the state along its Bloch-sphere trajectory to the north pole  $|E_1\rangle$  (up to a global phase). In the canonical qubit convention this is a  $\pi$ -rotation about  $\hat{y}$ , i.e.,  $R_y(\pi)$ , which flips  $|1\rangle \mapsto |0\rangle$  with an overall phase. The two descriptions are equivalent modulo phase and reflect the same geometric half-turn on  $S^2$  [25].

**Pauli-(Z)-type phase flip about the (z)-axis.** Let us consider the equal-norm superposition at  $kL = -\pi/2$ ,

$$\frac{|E_1\rangle + i|E_2\rangle}{\sqrt{2}},$$

which is taken by a  $z$ -axis phase flip to

$$\frac{|E_1\rangle - i|E_2\rangle}{\sqrt{2}}.$$

Within our basis convention this phase inversion is represented by

$$\begin{bmatrix} 0 & e^{i\pi} \\ 1 & 0 \end{bmatrix} \begin{pmatrix} -0.618i \\ 0.382 \end{pmatrix} = \begin{pmatrix} 0.382 \\ 0.618i \end{pmatrix},$$

which embodies the  $|E_2\rangle \mapsto -|E_2\rangle$  action (a  $\pi$ -rotation about  $\hat{z}$ ) while respecting the observed complex amplitudes at those  $k$ -points. In the canonical computational basis this is the familiar  $Z = \text{diag}(1, -1)$ , i.e., the phase-shift gate  $P(\pi)$ ; the off-diagonal representative used here differs by a unitary change of basis and by phase convention but generates the same Bloch-sphere rotation.

**Hadamard followed by  $S$  (quadrature) phase.** A particularly instructive sequence is the Hadamard transformation followed by a quadrature phase, written as

$$H = \frac{1}{\sqrt{2}} \begin{bmatrix} 1 & 1 \\ 1 & -1 \end{bmatrix}, \quad S = \begin{bmatrix} 0 & 1 \\ i & 1 \end{bmatrix}.$$

In our elastic-bit basis,  $H$  rotates a pole state (e.g.,  $|E_1\rangle$ ) to an equatorial superposition, while the subsequent  $S$  adjusts the relative quadrature between  $|E_1\rangle$  and  $|E_2\rangle$ , steering the state azimuthally on the sphere. In the canonical qubit convention,  $S$  is the pure phase  $P(\pi/2) = \text{diag}(1, i)$ ; the non-diagonal representative above captures the same azimuthal advance once the basis and band-dependent phases are accounted for. The net effect reproduces the equatorial quarter-turn standard in single-qubit control (Hadamard followed by a  $\pi/2$   $z$ -rotation).

The aforementioned algebra acquires a direct mechanical interpretation: in the static diatomic lattice, sweeping  $k$  across the Brillouin zone produces great-circle trajectories whose parity encodes the  $\{0, \pi\}$  Zak classes; under space-time modulation, sideband mixing enlarges the accessible region on  $S^2$ , enabling continuous paths between states such as  $(|E_1\rangle \pm i|E_2\rangle)/\sqrt{2}$  and their phase-flipped counterparts. This is precisely what is seen around hybridization points in Fig. 2, where the  $k$ -parametric evolution of  $(\hat{\alpha}, \hat{\beta})$  explores latitudes and longitudes rather than a single meridian; the transformation from  $(|E_1\rangle + i|E_2\rangle)/\sqrt{2}$  to  $(|E_1\rangle - i|E_2\rangle)/\sqrt{2}$  thereby realizes a  $Z$ -type gate continuously along the band. Because these gate-like maps are rotations on  $S^2$ , the enclosed solid angle controls the geometric phase accrued by the elastic state, in direct analogy with qubit holonomies. The present approach is distinctive in that it reconstructs the complex coefficients and manipulates the classical superposition state itself on the Bloch sphere—thereby demonstrating gate-level control without decoherence and without post-measurement statistics, a capability not found in earlier treatments of phononic analogues.

### 3.2.3 Geometric Phase Formalism for the Two-Level (Bloch-Sphere) Manifold

We next cast the geometric phase of the diatomic lattice into the canonical language of a two-level system. Any pure lattice state can be written on the Bloch sphere as

$$|\psi\rangle = \hat{\alpha}|E_1\rangle + \hat{\beta}|E_2\rangle; \quad \sqrt{|\hat{\alpha}|^2 + |\hat{\beta}|^2} = 1, \quad (9)$$

so that its evolution is completely specified by the spherical angles  $\theta(k) = 2 \arctan(|\hat{\beta}/\hat{\alpha}|)$  and  $\varphi(k) = \arg(\hat{\beta}) - \arg(\hat{\alpha})$ . In the effective three-dimensional Hamiltonian space  $\hat{H}(k)$  the adiabatic eigen-spinors are  $|+k\rangle$  and  $|-k\rangle$ ; choosing the usual gauge angle  $\varepsilon$  to fix the overall phase, one obtains

$$|+k\rangle = e^{i\varepsilon(\theta, \varphi)} \begin{pmatrix} \cos \frac{\theta(k)}{2} \\ e^{i\varphi(k)} \sin \frac{\theta(k)}{2} \end{pmatrix}, \quad \text{with } \varepsilon = \frac{\pi}{2} \quad (\text{convenient Bloch gauge}). \quad (10)$$

For a closed trajectory  $\zeta \subset \text{BZ}$ , the accumulated Zak phase is

$$\chi(\zeta) = \oint_{\zeta} A(k) dk, \quad A(k) = i \langle +k | \partial_k +k \rangle, \quad (11)$$

with the Berry vector (connection)

$$\mathbf{B}_V(k) = i \langle +k | \nabla_k | +k \rangle.$$

On a discretized Brillouin zone—essential for numerical work—the manifestly gauge-invariant "overlap" formula reads [21]:

$$\mathbf{B}_V(k_i) = \left( \cos \frac{\theta_i}{2}, e^{-i\varphi_i} \sin \frac{\theta_i}{2} \right) \begin{pmatrix} \cos \frac{\theta_{i+1}}{2} \\ e^{i\varphi_{i+1}} \sin \frac{\theta_{i+1}}{2} \end{pmatrix}, \quad (12)$$

$$\chi_{\text{disc}} = -\text{Im} \left\{ \ln \left[ \prod_{i=1}^{N_c} \mathbf{B}_V(k_i) \right] \right\}. \quad (13)$$

Equations (11)–(13) are the conventional geometric-phase expressions in both the continuum and discrete settings. In the continuum, the Berry connection reads  $A(k) = i \langle u_k | \partial_k u_k \rangle$  and the Zak (Berry) phase is its line integral over a closed loop in the Brillouin zone; on a discretized mesh the same object is evaluated as the imaginary part of the logarithm of the ordered product of nearest-neighbor overlaps. These are the forms we use in (11)–(13), and they coincide with established treatments of Berry/Zak phases and their lattice discretizations [23, 26, 27].

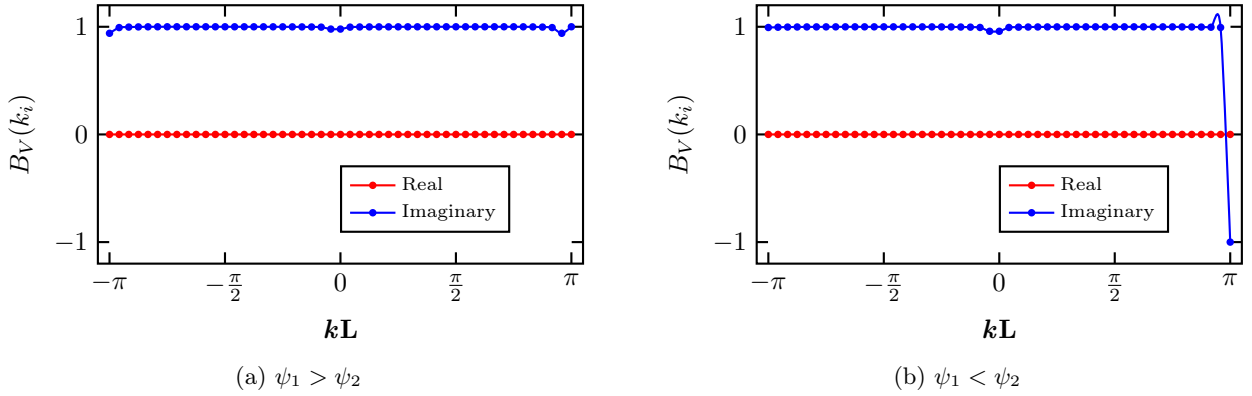


Figure 3: Analytical result of the real and imaginary component of the Berry vector corresponding to the stiffness of (a)  $\psi_1 > \psi_2$  and (b)  $\psi_1 < \psi_2$ .

With these definitions in hand, the unit-cell stiffness ordering fixes how the Bloch-sphere angles  $\theta(k)$  and  $\varphi(k)$  wind, and therefore how the geometric phase accumulates across the zone. The Berry vector extracted from Eq. (12) is purely imaginary in our data for both orderings (Figs. 3a–b), so the reported  $B_V(k)$  traces are controlled by their imaginary part. When  $\psi_1 > \psi_2$  [Fig. 3a],  $B_V(k)$  is essentially flat in  $k$ , leading to a vanishing line integral and a Zak phase of 0. When  $\psi_1 < \psi_2$  (Fig. 3b),  $B_V(k)$  changes sign once across the Brillouin zone, giving a net accumulation of  $\pi$ . This  $0/\pi$  dichotomy is the consequence of inversion symmetry in diatomic (SSH-type) chains and matches direct measurements of the Zak phase in one-dimensional lattices [8, 21].

The geometric content of Fig. 3 can be read directly on the Bloch sphere. When the state dwells near a pole ( $\theta \approx 0$  or  $\pi$ ), neighboring  $k$ -points have almost purely real and positive overlaps, so  $B_V(k)$  exhibits only small imaginary excursions and contributes negligibly to the total phase. By contrast, when the trajectory crosses the equator ( $\theta \approx \pi/2$ ), the azimuth  $\varphi$  winds rapidly; the overlaps acquire a large imaginary component, and the Zak phase picks up sharply. Varying the stiffness ratio (e.g.,  $\psi_1/\psi_2 = 2$  versus 0.5) shifts where  $\theta(k)$  and  $\varphi(k)$  vary most strongly, thereby relocating the  $k$ -intervals of enhanced Berry connection response. In other words, it is the twist of the state on the sphere—not its absolute location—that governs the geometric phase, in keeping with the general theory [26].

Seen through this lens, the Bloch sphere parameterization provides a compact and gauge-transparent narrative that is fully consistent with the spectral evaluation of the Berry/Zak phase via (11)–(13). In the two-mass case,  $\psi_1 > \psi_2$  yields a trivial loop with total twist  $\chi = 0$ , while  $\psi_1 < \psi_2$  yields a loop with a single twist  $\chi = \pi$ . This is precisely the classical-superposition analogue of the SSH chain’s inversion-protected  $0/\pi$  Zak-phase quantization: our diatomic lattice realizes the same binary topology, but the path lives on a classical Bloch sphere traced by the superposed modal amplitudes  $(\alpha, \beta)$ . The agreement between the Bloch sphere picture and the discretized-overlap evaluation in (12)–(13) reflects the robustness of gauge-invariant lattice formulas on discrete  $k$ -meshes [27].

Finally, we emphasize that SSH-type quantization of the Zak phase is well known in electronic, photonic, and ultracold-atom settings; however, in our system the same topological content is accessed and visualized through strictly classical superpositions on a Bloch sphere, with the stiffness ordering playing the role of dimerization. This qubit-like geometric representation—paired with a manifestly gauge-invariant numerical evaluation via (11)–(13)—provides a physically transparent bridge between classical elasticity and band-topological concepts, and it underpins the later extensions to multi-mass cells and spatiotemporal modulation developed in this manuscript [21, 26].

### 3.3 Three-Mass Unit Cell

We now consider a unit cell composed of three identical point masses that interact through linear, nearest-neighbor springs of stiffnesses  $\{\psi_1, \psi_2, \psi_3\}$ . Denoting by  $u_{n, N_i}(t)$  the displacement of mass  $n = 1, 2, 3$  in the  $N_i$ -th cell, the equations of motion read

$$\begin{aligned}
 m\ddot{u}_{1, N_i}(t) &= \psi_3 [u_{3, N_{i-1}}(t) - u_{1, N_i}(t)] - \psi_1 [u_{1, N_i}(t) - u_{2, N_i}(t)], \\
 m\ddot{u}_{2, N_i}(t) &= \psi_1 [u_{1, N_i}(t) - u_{2, N_i}(t)] - \psi_2 [u_{2, N_i}(t) - u_{3, N_i}(t)], \\
 m\ddot{u}_{3, N_i}(t) &= \psi_2 [u_{2, N_i}(t) - u_{3, N_i}(t)] - \psi_3 [u_{3, N_i}(t) - u_{1, N_{i+1}}(t)].
 \end{aligned}
 \tag{14}$$

These are solved with the Bloch ansatz.  $u_{n,N_i}(t) = A_n e^{ikN_i L} e^{i\omega t}$ . As in Sec. 3.1, we examine how inversion symmetry of the spring pattern controls whether the Zak (Berry) phase is quantized (0 or  $\pi$ ) or not. For a three-mass cell, inversion symmetry is the compact condition  $\psi_i = \psi_{N_m - i}$  with  $N_m = 3$ ; when it holds, the Zak phase of each isolated band is pinned to 0 or  $\pi \pmod{2\pi}$ —a standard result we will exploit below. Breaking inversion, by contrast, typically de-quantizes the geometric phase while leaving the spectrum invariant under origin shifts [18, 28]. To analyze intra-cell motion, it is convenient to resolve the displacement vector into the orthonormal basis

$$E_1 = \frac{1}{\sqrt{3}} \begin{bmatrix} 1 \\ 1 \\ 1 \end{bmatrix}, \quad E_2 = \frac{1}{\sqrt{2}} \begin{bmatrix} 1 \\ 0 \\ -1 \end{bmatrix}, \quad E_3 = \frac{1}{\sqrt{6}} \begin{bmatrix} 1 \\ -2 \\ 1 \end{bmatrix},$$

so that

$$\begin{bmatrix} u_{1,N_i}(t) \\ u_{2,N_i}(t) \\ u_{3,N_i}(t) \end{bmatrix} = \begin{bmatrix} A_1 \\ A_2 \\ A_3 \end{bmatrix} e^{ikN_i L} e^{i\omega t} \equiv (\alpha E_1 + \beta E_2 + \gamma E_3) e^{i\omega t}. \quad (15)$$

Here  $A_n$  are the traveling-wave amplitudes of the physical masses, while  $\alpha, \beta, \gamma$  are the complex modal coefficients in the internal basis  $\{E_1, E_2, E_3\}$ . To compare trends across bands and parameter sets, we rescale the modal coefficients by the band-resolved physical amplitudes through

$$\begin{aligned} \hat{\alpha} &= \frac{1}{|\operatorname{Re} A_1| + |\operatorname{Im} A_1|} \left( \frac{1}{\sqrt{3}} A_1 + \frac{1}{\sqrt{2}} A_2 + \frac{1}{\sqrt{6}} A_3 \right) e^{ikN_i L}, \\ \hat{\beta} &= \frac{1}{|\operatorname{Re} A_2| + |\operatorname{Im} A_2|} \left( \frac{1}{\sqrt{3}} A_1 - \frac{2}{\sqrt{6}} A_3 \right) e^{ikN_i L}, \\ \hat{\gamma} &= \frac{1}{|\operatorname{Re} A_3| + |\operatorname{Im} A_3|} \left( \frac{1}{\sqrt{3}} A_1 - \frac{1}{\sqrt{2}} A_2 + \frac{1}{\sqrt{6}} A_3 \right) e^{ikN_i L}. \end{aligned} \quad (16)$$

We study three representative stiffness sets:

$$(i) \psi_1 = \psi_2, \psi_3 = 2\psi_1; \quad (ii) \psi_1 = \psi_2, \psi_3 = \frac{1}{2}\psi_1; \quad (iii) \psi_2 = \psi_3, \psi_1 = 2\psi_2.$$

Cases (i)–(ii) satisfy inversion symmetry and therefore must yield Zak phases equal to 0 or  $\pi \pmod{2\pi}$ , while case (iii) explicitly breaks inversion and thus generically produces non-quantized geometric phases [18]. For each case, we compute the dispersion and the cell-wise complex amplitudes  $(\hat{\alpha}, \hat{\beta}, \hat{\gamma})$  across the Brillouin zone  $kL \in [-\pi, \pi]$ .

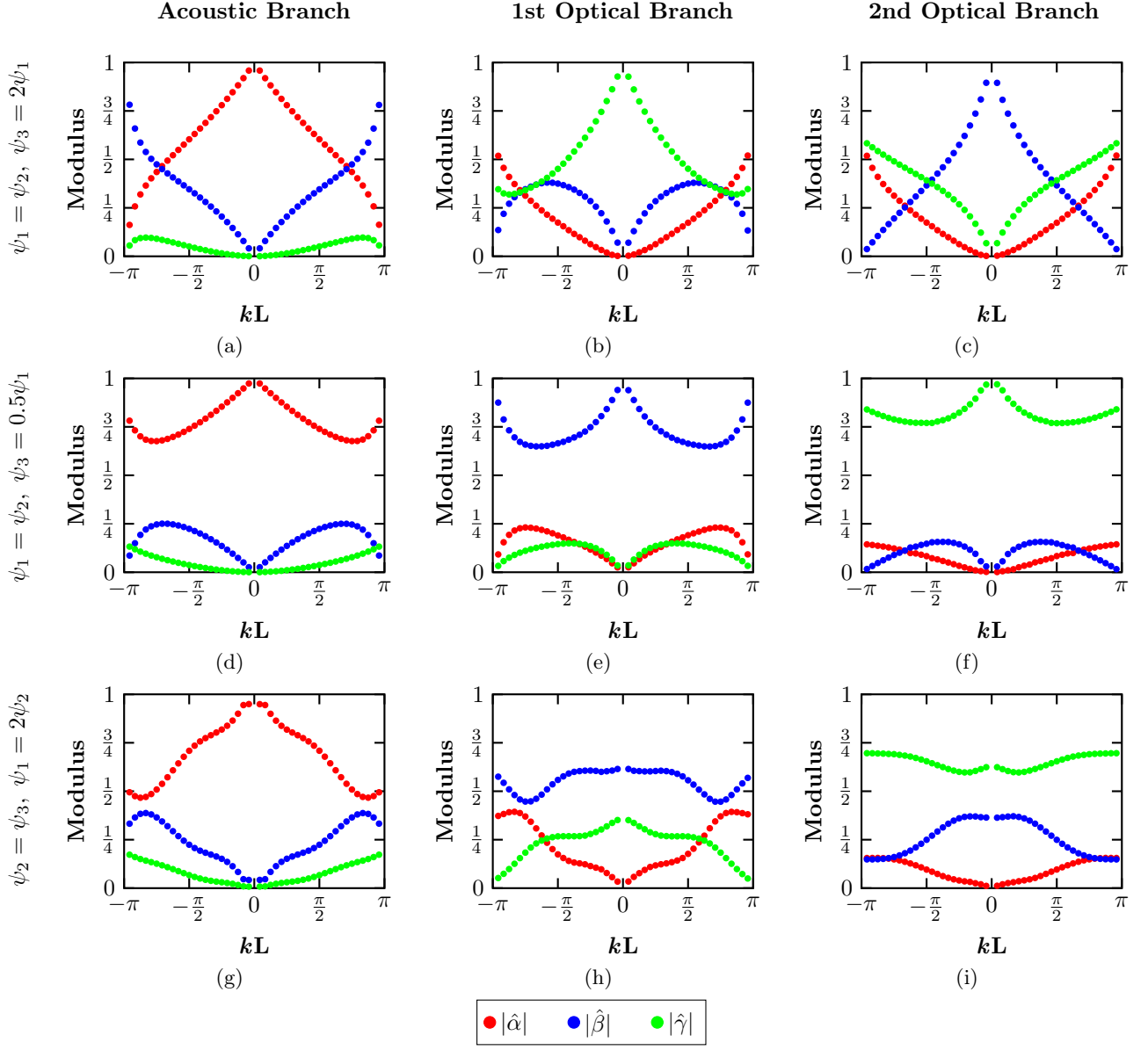


Figure 4: Evolution of the coefficients of the complex amplitude of a three mass unit cell at different set of parameters.

From Fig. 4, we see that the domination of the complex coefficients depends on the set of parameters. Across all three parameter sets, the acoustic branch is dominated by  $\hat{\alpha}$ . We can see an interchangeable effect in the 1st and 2nd optical branches in the case of the parameter set case (i)  $\psi_1 = \psi_2, \psi_3 = 2\psi_1$  and (ii)  $\psi_1 = \psi_2, \psi_3 = 0.5\psi_1$ . These two conditions of stiffness show a shift in the domination of the complex coefficients  $|\hat{\beta}|$  and  $|\hat{\gamma}|$ . This inversion in the 1st and 2nd optical shows a topological transition within the branches in the Hilbert space. And, across different parameters, we can see the clear separation of complex coefficients  $|\hat{\alpha}|$ ,  $|\hat{\beta}|$  and  $|\hat{\gamma}|$ . This clear separation—visible in Fig. 4 for cases (4c)–(4i)—provides an unambiguous, stiffness-agnostic labeling of the three branches that we will use to compare the phase evolution below. The continuity of these modulus trends through the Brillouin zone is also consistent with the smooth evolution of the Bloch eigenvectors away from high-symmetry points. We will focus on the acoustic branch for the set parameters.

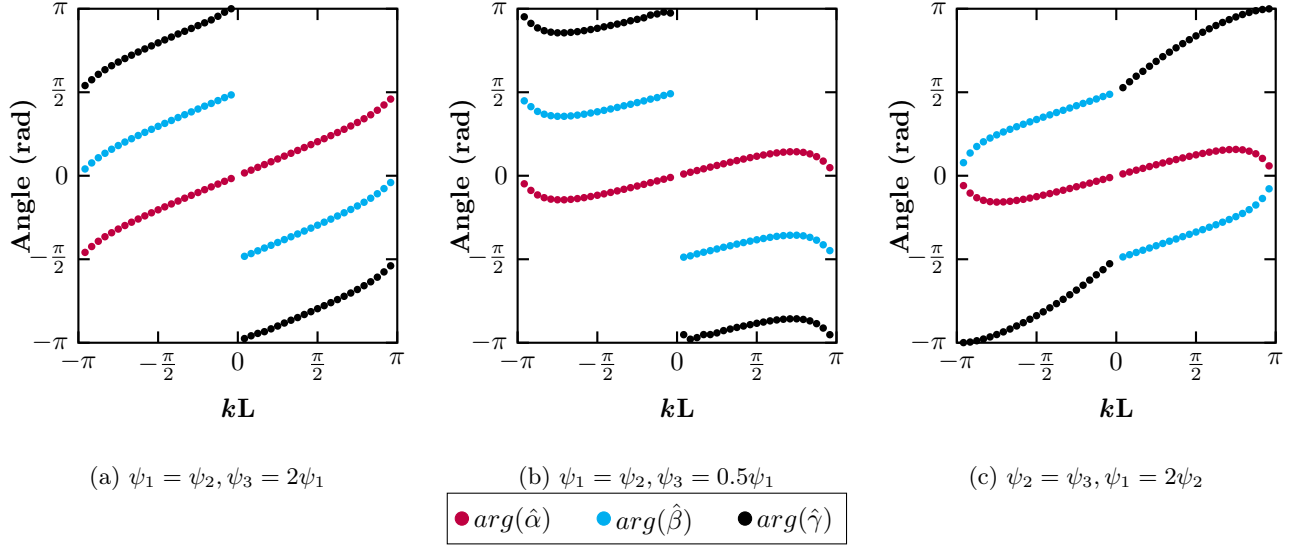


Figure 5: Absolute phases of the complex coefficients at the acoustic branch at the set parameters (i)  $\psi_1 = \psi_2, \psi_3 = 2\psi_1$ , (ii)  $\psi_1 = \psi_2, \psi_3 = 0.5\psi_1$ , and (iii)  $\psi_2 = \psi_3, \psi_1 = 2\psi_2$ .

When inversion symmetry is present, the pairwise phase differences of the dominant modal components are locked to constant offsets throughout each half zone, with discrete  $\pi$  flips at symmetry points. In our data,

$$\arg(\hat{\alpha}) - \arg(\hat{\beta}) \simeq -\frac{\pi}{2}, \quad \arg(\hat{\beta}) - \arg(\hat{\gamma}) \simeq +\frac{\pi}{2}$$

up to the expected jumps at  $kL = 0, \pm\pi$ . Further, the absolute phases  $\arg(\hat{\alpha})$ ,  $\arg(\hat{\beta})$ , and  $\arg(\hat{\gamma})$  show a single net  $\pi$  twist as  $k$  traverses the zone in the  $\pi$ -Zak case (Fig. 5a), whereas it exhibits either zero or two twists in the 0-Zak case (Fig. 5b). This  $\pi$ -twist counting is the same geometric diagnostic used for the two-mass cell (Sec. 3.1) and is precisely what the inversion-protected quantization of the Zak phase prescribes in one dimension [18, 29].

Breaking inversion symmetry destroys this rigid phase locking: in case (iii) the pairwise phase differences vary smoothly with  $k$  and are not pinned to  $\pm\pi/2$ ; the absolute phases  $\arg(\hat{\alpha})$ ,  $\arg(\hat{\beta})$ , and  $\arg(\hat{\gamma})$  show mixed slopes rather than coherent, single-twist trends (Fig. 5c). These behaviors—continuous drifts of relative and absolute phases and the loss of a well-defined  $\pi$ -twist count—are hallmarks of a non-quantized geometric phase [28].

Within the inversion-symmetric sets, the relative-phase fingerprints are similar, so a practical discriminator between the two Zak classes is the evolution of the absolute phases with  $k$ . In the  $\pi$ -Zak case (Fig. 5a) all three absolute phases increase monotonically over one traversal of the zone and host a single  $\pi$  twist located either at the zone center or at the boundaries. In the 0-Zak case (Fig. 5b) each absolute phase either drifts without net twist or executes two equal-and-opposite twists over a  $2\pi$  advance in  $k$ . This simple slope test—consistent with inversion-enforced quantization of the Berry phase in 1D lattices—proves useful for diagnosing topology directly from the measured modal phases [18].

Taken together, Fig. 4 and 5 encapsulates the central trends. (i) For inversion-symmetric triplets [(i)–(ii)] the Berry phase of each band is quantized (0 or  $\pi$ ), the modulus hierarchy  $|\hat{\alpha}|/|\hat{\beta}|/|\hat{\gamma}|$  cleanly labels the acoustic and optical branches, and the phase differences lock to  $\pm\pi/2$  with a single ( $\pi$ -Zak) or zero/two (0-Zak) twists per Brillouin-zone revolution. (ii) For the inversion-broken triplet [(iii)] the phase differences are unlocked and the absolute phases show mixed drifts—signatures of non-quantized, geometry-dependent Berry phases. These observations mirror the two-mass results and align with the general principle that 1D inversion symmetry pins the Zak phase to  $\{0, \pi\}$ , whereas breaking inversion allows it to vary continuously [28].

### 3.4 Bloch-Sphere Implications For a Three-Component State

The three-mass unit cell spans a three-component complex state  $\alpha|E_1\rangle + \beta|E_2\rangle + \gamma|E_3\rangle$  (up to an overall phase and normalization). Unlike a two-level system, which admits an  $S^2$  (Bloch-sphere) representation, there is no single sphere that globally parameterizes all pure three-level (qutrit-like) states. Instead, the natural

geometry is an eight-component generalized Bloch vector associated with  $SU(3)$ —often termed the “Bloch ball” for qutrits—or, equivalently, a set of pairwise two-level projections (e.g.,  $\{|E_1\rangle, |E_2\rangle\}$ ,  $\{|E_2\rangle, |E_3\rangle\}$ ,  $\{|E_1\rangle, |E_3\rangle\}$ ), each of which maps to a standard Bloch sphere [30, 31].

Within this viewpoint, the phase locking observed under inversion,  $\arg(\hat{\alpha}) - \arg(\hat{\beta}) = \pm \frac{\pi}{2}$  and  $\arg(\hat{\beta}) - \arg(\hat{\gamma}) = \mp \frac{\pi}{2}$ , implies that each pairwise projection traces an arc of constant latitude/longitude on its corresponding Bloch sphere as  $k$  winds through the Brillouin zone, with the total azimuthal change encoding an odd ( $\pi$ -Zak) or even (0-Zak) number of  $\pi$  twists. The three-level trajectory therefore decomposes into three mutually consistent two-sphere paths whose parity (odd vs. even twist) matches the bulk Zak class. When inversion is broken, these projected paths depart from great-circle arcs, and components of the  $SU(3)$  Bloch vector no longer integrate to a quantized Berry phase—precisely what the unlocked,  $k$ -dependent phase differences in Fig. 5c convey [30, 32].

In summary, the present section advances beyond prior analyses by (i) demonstrating, in a classical three-degree-of-freedom setting, robust superpositions whose evolution on pairwise Bloch spheres reproduces the  $\{0, \pi\}$  topology of inversion-symmetric bands and (ii) explicitly connecting those trajectories to a generalized  $SU(3)$  Bloch-vector picture that has, to date, been discussed mainly in quantum contexts. In this sense, the three-mass cell functions as a minimal mechanical platform where classical superpositions emulate quantum-state kinematics, and where the Berry/Zak phase can be read directly from the geometry of the projected Bloch-sphere paths—providing a direct bridge between mechanical waves and geometric-phase ideas from condensed-matter and quantum information theory [26, 30].

## 4 Lattice with Time-Dependent Stiffness

### 4.1 Two-Mass System

To extend the static analysis, we examine the same diatomic elastic lattice when the two masses are coupled by springs whose stiffness is modulated sinusoidally in both space and time.

To compute the dispersion and to extract complex amplitudes and phases for each branch, we use a two-step MD  $\rightarrow$  SAAP workflow (see Supplementary Material, similar to [10]): first determine  $\omega_j(k)$  from random-phase excitation; then re-excite each band with traveling-wave initial conditions to extract complex amplitudes and phases, and finally project onto  $\{|E_1\rangle, |E_2\rangle\}$  to obtain  $\alpha(k), \beta(k)$ . In the first series of MD runs, the modulation (phase) velocity is fixed at  $V_m = 350$  m/s. For each wave number, we analyze two modulation patterns, denoted  $\psi_n^+$  and  $\psi_n^-$  (definitions below). The modulation of the force constant adopts the form introduced earlier in Eq. (1) and implemented previously in SAAP-based studies of spatiotemporal lattices, where two MD passes with carefully chosen initial conditions are required to resolve both the frequencies and the phases of the traveling modes. In particular, the second MD pass must employ traveling-wave initial conditions to avoid arbitrary phase offsets—an essential distinction between SAAP and eigenvector-only approaches. Specifically,

$$\psi_n(t) = \psi_0 \pm \Delta\psi \sin(k_m x_n - \omega_m t), \quad (17)$$

where  $\psi_0$  is the baseline stiffness,  $\Delta\psi$  the modulation amplitude, and  $k_m$  and  $\omega_m$  the modulation wave number and angular frequency, respectively. Introducing the spatial period  $\lambda_m = 2\pi/k_m = L = N_m a$  (with inter-mass spacing  $a$ ), we may equivalently write

$$\psi_n(t) = \psi_0 \pm \Delta\psi \sin\left(\frac{2\pi(x_n - V_m t)}{L}\right). \quad (18)$$

We label  $\psi_n^+$  for the “+” and  $\psi_n^-$  for the “−” choice. These two cases are related by an origin shift of half a cell (from the first mass to mid-cell).

Consequently, they share the same band structure but differ by Berry-phase conventions tied to origin choice—an invariance of the spectrum under unitary re-labelings that simultaneously allows different Berry phases under translations of the real-space origin [10].

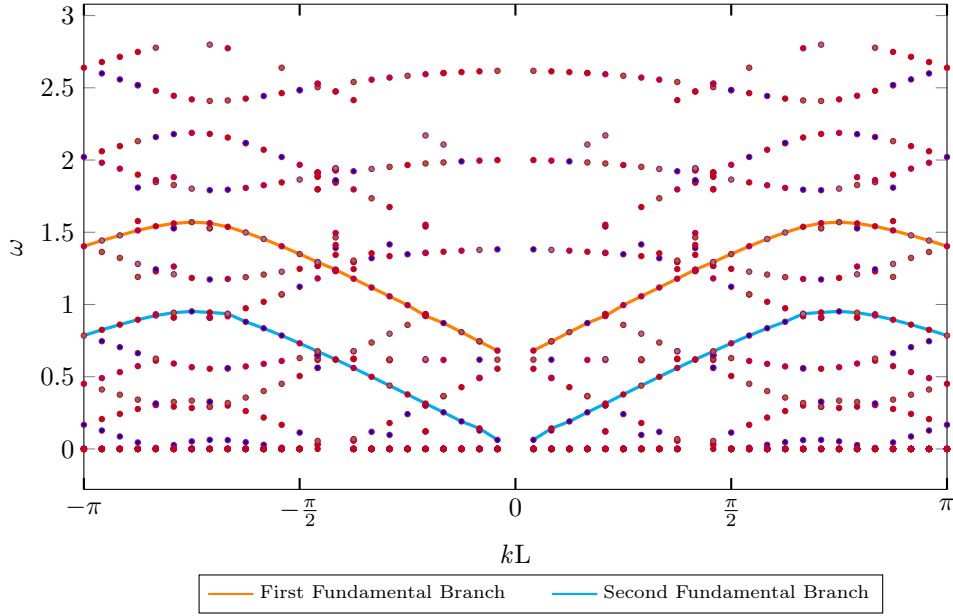


Figure 6: Elastic wave band structure for variable periodical sinusoidal modulation of stiffness at  $V_m = 350m/s$ . The red line defines the first fundamental branch, and the green line represents the second one.

Fig. 6 shows the dispersion of the space-time-modulated superlattice (as also reported in our prior work on [11]). The moving modulation generates directional hybridization (one-sided) gaps and Doppler-shifted replicas of the static branches—canonical signatures of non-reciprocal phononic media with space-time periodicity and Willis-type effective descriptions. The placement and multiplicity of gaps depend on the modulation speed and harmonic content, consistent with general theories and with beam-lattice implementations of spatiotemporal elasticity [9, 33, 34].

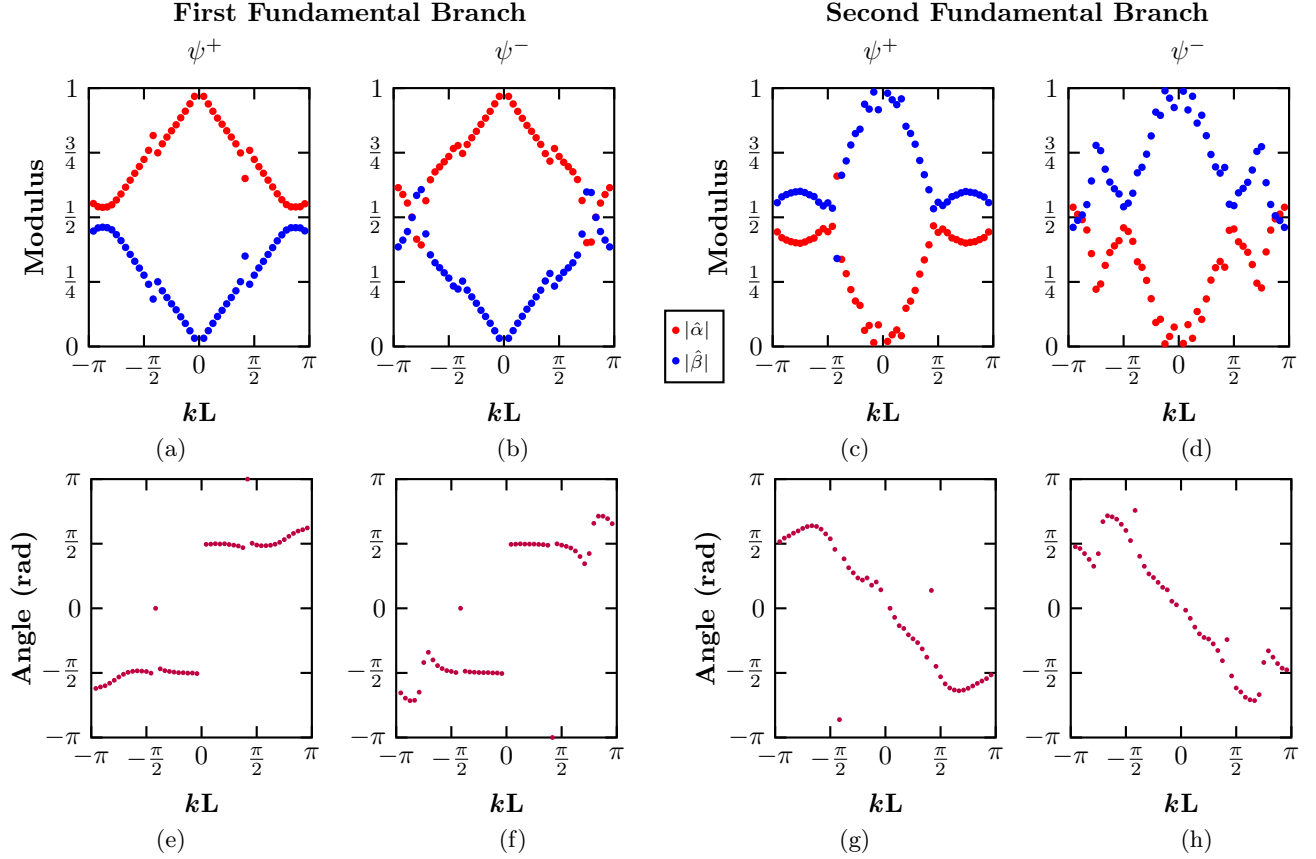


Figure 7: Amplitude and Phase modulation of the two-mass system for the time-dependent stiffness of the harmonic spring for the stiffness of  $\psi^+$  and  $\psi^-$  at the first (FFB) and second (SFB) fundamental branch. **Top Panel:** Modulus of complex amplitudes  $|\hat{\alpha}|$  and  $|\hat{\beta}|$ . **Bottom Panel:** Phase difference between the amplitude moduli  $\arg(\hat{\alpha}) - \arg(\hat{\beta})$ .

From the second set of MD simulations with traveling-wave initial conditions, we extract the complex superposition coefficients in the two-state in-cell basis  $(\hat{\alpha}, \hat{\beta})$  exactly as in the static case. Relative to the time-independent lattice, the modulation sharpens the  $k$ -dependence of both moduli and phases (Fig. 7). Most notably, the relative phase  $\Delta\phi = \arg(\hat{\alpha}) - \arg(\hat{\beta})$  is no longer piecewise constant: it winds across the Brillouin zone as carrier harmonics mix with Floquet sidebands, whereas in the static lattice inversion symmetry pins  $\Delta\phi$  to  $\{-\pi/2, +\pi/2\}$  on intervals separated by  $\pi$ -jumps at high-symmetry points. The modulus hierarchy on the FFB largely mirrors the static case— $|\hat{\alpha}| > |\hat{\beta}|$  over wide  $k$ -intervals—yet the  $\psi^+$  and  $\psi^-$  patterns differ by origin-dependent flips that track the  $0/\pi$  swapping induced by unit-cell translations. Under temporal modulation, this swapping persists but the geometric phase becomes open-path: it is accumulated along the actual FFB trajectory in  $k$  and does not require a closed loop. This is precisely the Samuel-Bhandari generalization of the Berry phase to non-cyclic evolution [5].

On the SFB, the coefficient roles invert relative to the FFB:  $|\hat{\beta}|$  becomes dominant over extended  $k$ -ranges and  $\Delta\phi(k)$  exhibits larger excursions with alternating increases and decreases across the hybridization regions (Fig. 7). This behavior is expected because the SFB approaches—and in places crosses—additional hybridization points where Brillouin harmonics intersect the folded static bands, producing sharp kinks or discrete jumps in both amplitude and phase. The emergence and placement of these discontinuities with increasing modulation velocity are consistent with our prior perturbative estimates and with published analyses of spatiotemporally modulated elastic lattices [33].

Taken together, these results lead to three conclusions germane to the manuscript’s central thesis. First, the moving stiffness modulation preserves branch identification (FFB vs. SFB) and the equivalence of  $\psi^+$  and  $\psi^-$  up to an origin shift, but it qualitatively alters the evolution of  $\Delta\phi(k)$ : the piecewise-constant behavior of the static chain is replaced by a modulation-induced winding (Fig. 7). Second, the Berry-phase convention

associated with origin choice (0 for  $\psi^+$ ,  $\pi$  for  $\psi^-$ ) endures under temporal modulation, now interpreted as an open-path geometric phase—precisely the scenario anticipated by non-cyclic geometric-phase theory and verified numerically in our earlier work on *Geometric-phase invariance*. Third, the Bloch-sphere trajectories expand from nearly planar arcs to fully three-dimensional loops, reflecting multi-harmonic coupling and enabling classical superpositions that operate like qubit rotations on the Bloch sphere. This geometric, coefficient-level description is the distinctive contribution of the present manuscript compared with prior studies of non-reciprocal elastic media: here, the band eigenstates are explicitly cast and measured as classical superpositions whose trajectories on the Bloch sphere make the corresponding Berry/Zak phases—closed or open—directly visible and origin-aware. That synthesis dovetails with foundational treatments of space-time modulation in phononic crystals and Willis materials, and it clarifies how directional gaps and Doppler-shifted replicas coexist with robust geometric-phase assignments in time-dependent lattices [9, 33].

## Bloch-Sphere Picture With Time-Dependent Stiffness

The Bloch-sphere representation remains a powerful geometric lens for the two-mass cell. With static stiffness, the state vector traces an approximate circle (one “plane” on the sphere) as  $k$  sweeps the zone. Under space-time modulation, the extra quadratures generated by sideband mixing allow the state to explore a much larger portion of the sphere—sampling both longitudes and latitudes rather than remaining confined to a single great-circle arc (Fig. 8). Physically, near hybridization points the instantaneous diatomic state admits admixtures that effectively span the full two-state manifold, and the accumulated geometric phase follows the non-cyclic, geodesically closed prescription [5].

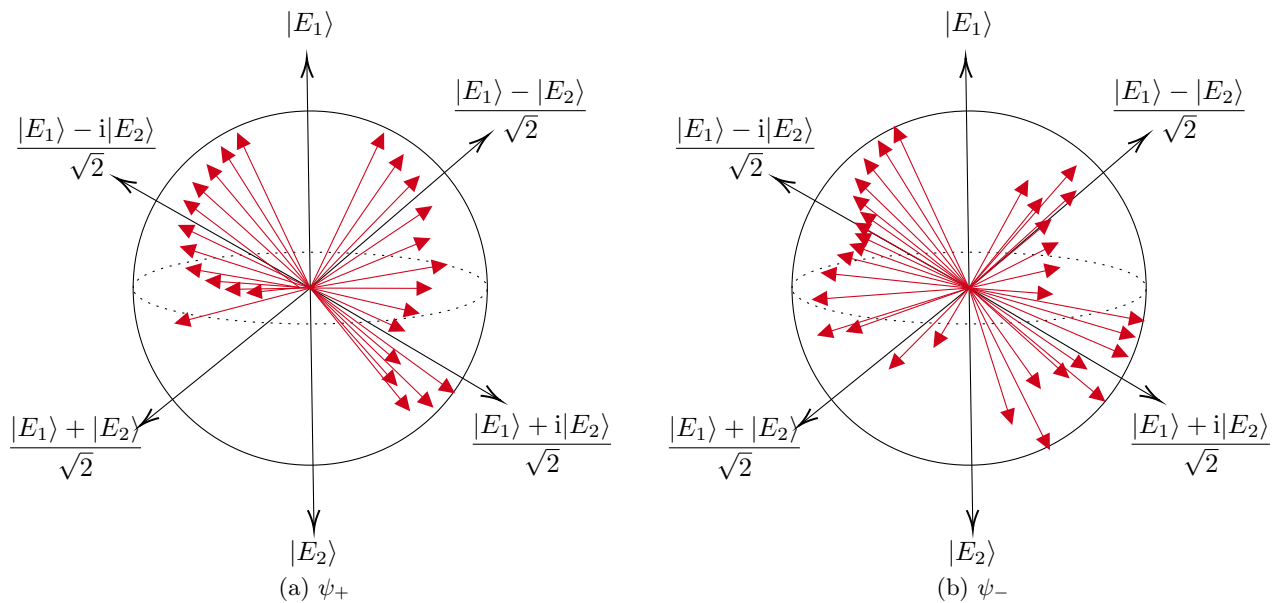


Figure 8: Bloch state demonstration of change of state between  $|E_1\rangle$  and  $|E_2\rangle$  at a two-mass system depicted in Hilbert Space with different stiffness matrices for the two cases (a)  $\psi^+$  (b)  $\psi^-$  at the FFB.

Figure 8 represents the Bloch state in the spatiotemporal modulation’s FFB. Unlike the previous case, where the stiffness is independent of time and one direction, Bloch states are explored. We can analyze much larger regions of the Bloch states by switching to time-dependent stiffness of the lattices. The modulus hierarchy  $|\hat{\alpha}| > |\hat{\beta}|$  on the  $k$  band indicates that the states are approaching the pure state  $|E_1\rangle$ . However, the random change in relative phase ( $\arg(\hat{\alpha}) - \arg(\hat{\beta})$ ) indicates a state approach that deviates from the straight path as before.

The Bloch-state representation further enables the realization of quantum-analogous gate operations. For example, as illustrated in Fig. 8b, the state  $(|E_1\rangle + i|E_2\rangle)/\sqrt{2}$  can be transformed into  $(|E_1\rangle - i|E_2\rangle)/\sqrt{2}$  by an operation analogous to the Pauli- $Z$  gate, which effectively maps  $|E_2\rangle \rightarrow -|E_2\rangle$ . In the elastic lattice, this transformation can be traced continuously through the  $k$ -space sweep of the band structure, demonstrating that state manipulation on the Bloch sphere has a direct counterpart in the underlying mechanical system.

Whereas earlier work established non-reciprocity and hybridization in space-time modulated lattices, the present treatment reconstructs the classical superposition state itself—via SAAP—from MD data and represents its  $k$ -parametric evolution on the Bloch sphere. This provides a physically transparent, gauge-clean route to Berry/Zak phases (including their origin dependence) in both static and time-modulated settings, thereby demonstrating a classical analogue of qubit control that to our knowledge has not been articulated in this coefficient-level, Bloch-sphere form for diatomic elastic chains.

## 5 Concluding Remarks

We have developed and validated a compact, superposition-based description of one-dimensional elastic lattices that makes their band topology visible and computable directly from amplitude–phase data. We recast intra-cell vibrations of the elastic lattice into normalized combinations of orthogonal eigenstates and tracked the corresponding complex coefficients across the Brillouin zone. In the lattice with time-independent stiffness, this led to a two-level (spinor) representation for diatomic chains in which the relative phase between the in-phase and out-of-phase modes is locked by inversion symmetry, yielding the expected quantization of the Zak phase to 0 or  $\pi$ . Extending the framework to triatomic cells showed how breaking inversion symmetry de-quantizes the individual band phases while preserving global constraints (e.g., band-sum invariants), clarifying which features are symmetry-protected and convention-dependent. Within this same static, two-level picture, we also operationalizes the geometry by casting norm-preserving transformations of the coefficient pair  $(\hat{\alpha}, \hat{\beta})$  as  $SU(2)$  rotations on the Bloch sphere, i.e., quantum-analogue gates in a classical lattice—with explicit examples such as a  $y$ -axis  $\pi$ -rotation that flips between  $|E_2\rangle$  and  $|E_1\rangle$  and  $z$ -axis phase inversions of balanced superpositions. This gate viewpoint supplies an explicit, basis-aware language for state manipulation (up to overall phase conventions) and reframes our Bloch-sphere trajectories as controllable rotations rather than merely descriptive curves, strengthening the link between classical lattice dynamics and qubit kinematics.

A second principal outcome arises when a lattice with time-dependent stiffness is introduced via a moving spatiotemporal modulation of the elastic stiffness. Two robust qualitative changes appear. First, the static, piecewise-constant behavior of the relative phase is replaced by a modulation-induced winding across  $k$ , reflecting hybridization between carrier harmonics and Floquet sidebands; second, the Berry phase ceases to be defined only for closed  $k$ -loops and is instead realized as an open-path geometric phase accumulated along the actual (Floquet) trajectory—precisely the Samuel–Bhandari generalization of Berry’s phase. In this regime, the Bloch-sphere trajectories expanded from nearly planar arcs to genuinely three-dimensional loops, providing a classical picture of qubit-like rotations driven by space–time coupling while preserving branch identification and the origin-dependent  $0/\pi$  exchange familiar from the static chain. These findings link geometric phase, modulation, and symmetry in a single, experimentally tractable language.

These results highlight the distinctive contribution of this manuscript relative to prior work. First, rather than inferring Berry/Zak phases from inner products of eigenvectors, we construct the state vector itself, band by band, and follow its evolution on the Bloch sphere; this makes quantization from inversion symmetry (0 or  $\pi$ ) transparent in diatomic lattices, and it provides a direct geometric rationale for the appearance of arbitrary (de-quantized) phases once that symmetry is broken in triatomic lattices. Second, the same construction remains valid under temporal modulation and naturally yields open-path phases, extending the analysis beyond periodic, adiabatic settings without introducing gauge ambiguities. Third, by articulating the quantum-analogue gate interpretation, the framework not only visualizes but also prescribes  $SU(2)$ -equivalent rotations in a classical medium, thereby clarifying how plateaus, jumps, and windings in relative phase map to actionable operations on the sphere—and, in the time-modulated setting, how such operations extend along non-cyclic loops. Together, these contributions move beyond earlier amplitude–phase spectroscopy to a Hilbert-space viewpoint that is compact and applicable to static and time-varying media.

**Acknowledgements** M.A.H. acknowledges partial support from NSF Grant No. 2204382. This work was also supported by the Science and Technology Center New Frontiers of Sound (NewFoS) through NSF Grant No. 2242925.

**Author Contributions** M.A.H. conceived the idea of the research. All authors analyzed the findings and contributed to the scientific discussion and the manuscript's writing.

**Competing Interests** The authors declare no competing interests.

**Data Availability Statement** The data that support our findings of the present study are available from the corresponding author upon reasonable request.

## References

- [1] Pierre A. Deymier and Keith Runge. *Sound Topology, Duality, Coherence and Wave-Mixing: An Introduction to the Emerging New Science of Sound*. Vol. 188. Springer Series in Solid-State Sciences. Springer, 2017. DOI: 10.1007/978-3-319-62380-1.
- [2] Sebastian D. Huber. “Topological mechanics”. In: *Nature Physics* 12 (2016), pp. 621–623. DOI: 10.1038/nphys3801.
- [3] J. Zak. “Berry’s phase for energy bands in solids”. In: *Phys. Rev. Lett.* 62 (23 June 1989), pp. 2747–2750. DOI: 10.1103/PhysRevLett.62.2747.
- [4] Shinsei Ryu and Yasuhiro Hatsugai. “Topological Origin of Zero-Energy Edge States in Particle-Hole Symmetric Systems”. In: *Phys. Rev. Lett.* 89 (7 July 2002), p. 077002. DOI: 10.1103/PhysRevLett.89.077002.
- [5] Joseph Samuel and Rajendra Bhandari. “General Setting for Berry’s Phase”. In: *Phys. Rev. Lett.* 60 (23 June 1988), pp. 2339–2342. DOI: 10.1103/PhysRevLett.60.2339.
- [6] C. L. Kane and T. C. Lubensky. “Topological boundary modes in isostatic lattices”. In: *Nature Physics* 10.1 (2014), pp. 39–45. DOI: 10.1038/nphys2835.
- [7] S. Hossein Mousavi, Alexander B. Khanikaev, and Zheng Wang. “Topologically protected elastic waves in phononic metamaterials”. In: *Nature Communications* 6 (2015), p. 8682. DOI: 10.1038/ncomms9682.
- [8] C. Liu, H. R. Wang, and H. C. Ong. “Determination of the Zak phase of one-dimensional diffractive systems with inversion symmetry via radiation in Fourier space”. In: *Phys. Rev. B* 108 (3 July 2023), p. 035403. DOI: 10.1103/PhysRevB.108.035403.
- [9] H. Nassar et al. “Non-reciprocal wave propagation in modulated elastic metamaterials”. In: *Proceedings of the Royal Society A: Mathematical, Physical and Engineering Sciences* 473.2202 (2017), p. 20170188. DOI: 10.1098/rspa.2017.0188.
- [10] M. Arif Hasan et al. “Spectral analysis of amplitudes and phases of elastic waves: Application to topological elasticity”. In: *The Journal of the Acoustical Society of America* 146.1 (July 2019), pp. 748–766. DOI: 10.1121/1.5114911.
- [11] M. Arif Hasan et al. “Geometric phase invariance in spatiotemporal modulated elastic system”. In: *Journal of Sound and Vibration* 459 (2019), p. 114843. DOI: 10.1016/j.jsv.2019.07.009.
- [12] J.B. Altepeter, E.R. Jeffrey, and P.G. Kwiat. “Photonic State Tomography”. In: *Advances In Atomic, Molecular, and Optical Physics* 52 (2005). Ed. by P.R. Berman and C.C. Lin, pp. 105–159. ISSN: 1049-250X. DOI: 10.1016/S1049-250X(05)52003-2.
- [13] Omar Gamel and Daniel F. V. James. “Measures of quantum state purity and classical degree of polarization”. In: *Phys. Rev. A* 86 (3 Sept. 2012), p. 033830. DOI: 10.1103/PhysRevA.86.033830.
- [14] Filippo Cardano et al. “Detection of Zak phases and topological invariants in a chiral quantum walk of twisted photons”. In: *Nature Communications* 8.1 (2017), p. 15516. DOI: 10.1038/ncomms15516.
- [15] Stefano Longhi. “Zak phase of photons in optical waveguide lattices”. In: *Opt. Lett.* 38.19 (Oct. 2013), pp. 3716–3719. DOI: 10.1364/OL.38.003716.
- [16] János K Asbóth, László Oroszlány, and András Pályi. *A short course on topological insulators*. Vol. 919. Springer, 2016.
- [17] Michael Victor Berry. “Quantal phase factors accompanying adiabatic changes”. In: *Proceedings of the Royal Society of London. A. Mathematical and Physical Sciences* 392.1802 (1984), pp. 45–57. DOI: 10.1098/rspa.1984.0023.
- [18] Zhi-Qiang Jiao et al. “Experimentally Detecting Quantized Zak Phases without Chiral Symmetry in Photonic Lattices”. In: *Phys. Rev. Lett.* 127 (14 Sept. 2021), p. 147401. DOI: 10.1103/PhysRevLett.127.147401.
- [19] Kazi T. Mahmood and M. Arif Hasan. “Topological insights from state manipulation in a classical elastic system”. In: *AIP Advances* 15.2 (Feb. 2025), p. 025305. ISSN: 2158-3226. DOI: 10.1063/5.0245354.
- [20] Heejin Choi et al. “Phase of Topological Lattice with Leaky Guided Mode Resonance”. In: *Nanomaterials* 13.24 (2023), p. 3152. DOI: 10.3390/nano13243152.

- [21] Marcos Atala et al. “Direct measurement of the Zak phase in topological Bloch bands”. In: *Nature Physics* 9.12 (2013), pp. 795–800. DOI: 10.1038/nphys2801.
- [22] Meng Xiao, Z. Q. Zhang, and C. T. Chan. “Surface Impedance and Bulk Band Geometric Phases in One-Dimensional Systems”. In: *Phys. Rev. X* 4 (2 Apr. 2014), p. 021017. DOI: 10.1103/PhysRevX.4.021017.
- [23] G. P. Mikitik and Yu. V. Sharlai. “Manifestation of Berry’s Phase in Metal Physics”. In: *Phys. Rev. Lett.* 82 (10 Mar. 1999), pp. 2147–2150. DOI: 10.1103/PhysRevLett.82.2147.
- [24] Guangzhen Li et al. “Direct extraction of topological Zak phase with the synthetic dimension”. In: *Light: Science & Applications* 12.1 (2023), p. 81. ISSN: 2047-7538. DOI: 10.1038/s41377-023-01126-1.
- [25] Gavin E Crooks. „*Quantum Gates* “. 2024.
- [26] Di Xiao, Ming-Che Chang, and Qian Niu. “Berry phase effects on electronic properties”. In: *Rev. Mod. Phys.* 82 (3 July 2010), pp. 1959–2007. DOI: 10.1103/RevModPhys.82.1959.
- [27] Takahiro Fukui, Yasuhiro Hatsugai, and Hiroshi Suzuki. “Chern numbers in discretized Brillouin zone: Efficient method of computing (spin) Hall conductances”. In: *Journal of the Physical Society of Japan* 74.6 (2005), pp. 1674–1677. DOI: 10.1143/JPSJ.74.1674.
- [28] Yi-Xin Xiao, Zhao-Qing Zhang, and C. T. Chan. “Coexistence of quantized and non-quantized geometric phases in quasi-one-dimensional systems without inversion symmetry”. In: *arXiv preprint* (2016). arXiv:1605.00549.
- [29] Stefano Longhi. “Probing one-dimensional topological phases in waveguide lattices with broken chiral symmetry”. In: *Optics Letters* 43.19 (2018), pp. 4639–4642. DOI: 10.1364/OL.43.004639.
- [30] Gen Kimura. “The Bloch vector for N-level systems”. In: *Physics Letters A* 314.5 (2003), pp. 339–349. ISSN: 0375-9601. DOI: 10.1016/S0375-9601(03)00872-4.
- [31] Christopher Eltschka et al. “The shape of higher-dimensional state space: Bloch-ball analog for a qutrit”. In: *Quantum* 5 (2021), p. 485.
- [32] Cameron J. D. Kemp, Nigel R. Cooper, and F. Nur Ünal. “Nested-sphere description of the  $N$ -level Chern number and the generalized Bloch hypersphere”. In: *Phys. Rev. Res.* 4 (2 May 2022), p. 023120. DOI: 10.1103/PhysRevResearch.4.023120.
- [33] G Trainiti and M Ruzzene. “Non-reciprocal elastic wave propagation in spatiotemporal periodic structures”. In: 18.8 (Aug. 2016), p. 083047. DOI: 10.1088/1367-2630/18/8/083047.
- [34] H. Nassar et al. “Non-reciprocal flexural wave propagation in a modulated metabeam”. In: *Extreme Mechanics Letters* 15 (2017), pp. 97–102. ISSN: 2352-4316. DOI: 10.1016/j.eml.2017.01.012.

# Supplementary Materials

## S.1 Traveling Wave Solution in the Unit Cell

We first consider a system of two identical masses per unit cell with spring constants modulation for which the analytical solutions of the eigen-problem are available and can be compared with numerical results obtained via SAAP. Figure S1 represents the schematic of the 1D elastic lattices.

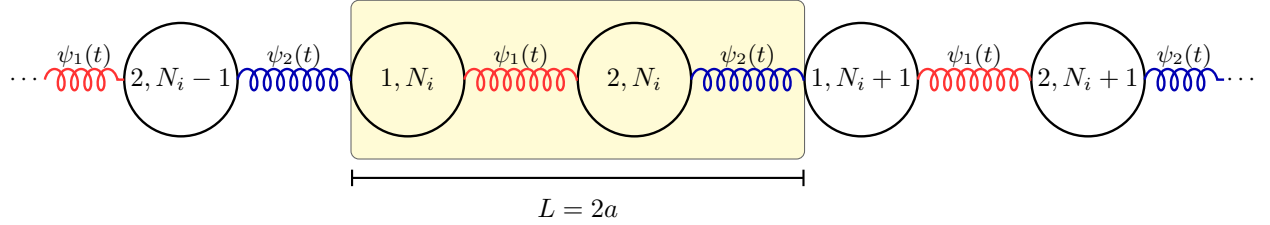


Figure S1: Schematic of a one-dimensional diatomic mass–spring lattice consisting of two identical masses per unit cell and alternating spring constants. Each unit cell of length  $L = 2a$  contains two masses,  $(1, N_i)$  and  $(2, N_i)$ , coupled by springs with stiffness  $\psi_1(t)$  and  $\psi_2(t)$ .  $a$  is the inter-mass spacing. The shaded region highlights a representative unit cell of the periodic structure.

### S.1.1 Two-Mass Unit Cell

The traveling wave solution of the Eq. (1) using the compact ansatz of Eq. (2) realizes that the amplitude  $A_n$  are periodical in reciprocal space. That is also in contrast to the Ansatz of the general form  $u_n = A'_n e^{ikx_n} e^{ikN_i L} e^{i\omega t}$ , where  $A'_n e^{ikx_n}$  is periodic in reciprocal space. We note that both ansatz are related by a unitary transformation that yields the same spectrum. Plugging in the Eq. (2) in Eq. (1) gives us the equation of motion as,

$$\begin{aligned} (-m\omega^2 + \psi_1 + \psi_2)A_1 - (\psi_1 + \psi_2 e^{-ikL})A_2 &= 0 \\ -(\psi_1 + \psi_2 e^{+ikL})A_1 + (-m\omega^2 + \psi_1 + \psi_2)A_2 &= 0 \end{aligned}$$

These form a set of linear equations in the amplitudes  $A_1$  and  $A_2$ . These can be rearranged in matrix form:

$$\begin{pmatrix} \gamma & -\tau^* \\ -\tau & \gamma \end{pmatrix} \begin{pmatrix} A_1 \\ A_2 \end{pmatrix} = \begin{pmatrix} 0 \\ 0 \end{pmatrix} \quad (\text{s1})$$

Here, we have defined  $\gamma = -m\omega^2 + \psi_1 + \psi_2$  and  $\tau = \psi_1 + \psi_2 e^{ikL}$ , where  $\tau^*$  denotes the complex conjugate of  $\tau$ . The nontrivial solutions lead to:

$$\gamma^2 - \tau\tau^* = 0 \quad \Rightarrow \quad \gamma = \pm\sqrt{\tau\tau^*}$$

Nontrivial solutions require the determinant to vanish:

$$\begin{aligned} &(\psi_1 + \psi_2 - m\omega^2)^2 - (\psi_1 + \psi_2 e^{-ikL})(\psi_1 + \psi_2 e^{ikL}) = 0 \\ \Rightarrow &[(\psi_1 + \psi_2)^2 - 2(\psi_1 + \psi_2)m\omega^2 + m^2\omega^4] - [\psi_1^2 + \psi_1\psi_2(e^{ikL} + e^{-ikL}) + \psi_2^2] = 0 \\ \Rightarrow &m^2\omega^4 - 2(\psi_1 + \psi_2)m\omega^2 + (\psi_1 + \psi_2)^2 - \psi_1^2 - \psi_2^2 - \psi_1\psi_2(e^{ikL} + e^{-ikL}) = 0 \\ \Rightarrow &m^2\omega^4 - 2(\psi_1 + \psi_2)m\omega^2 + (\psi_1 + \psi_2)^2 - \psi_1^2 - \psi_2^2 - 2\psi_1\psi_2 \cos(kL) = 0 \\ \Rightarrow &m^2\omega^4 - 2(\psi_1 + \psi_2)m\omega^2 + [\psi_1^2 + 2\psi_1\psi_2 + \psi_2^2 - \psi_1^2 - \psi_2^2 - 2\psi_1\psi_2 \cos(kL)] = 0 \\ \Rightarrow &m^2\omega^4 - 2(\psi_1 + \psi_2)m\omega^2 + 2\psi_1\psi_2(1 - \cos kL) = 0 \\ \Rightarrow &m^2\omega^4 - 2(\psi_1 + \psi_2)m\omega^2 + 4\psi_1\psi_2 \sin^2\left(\frac{kL}{2}\right) = 0, \quad \left[1 - \cos kL = 2 \sin^2\left(\frac{kL}{2}\right)\right] \end{aligned}$$

which is a quadratic equation for  $\omega^2$ . Solving,

$$\omega_{\pm}^2 = \frac{\psi_1 + \psi_2}{m} \left[ 1 \pm \sqrt{1 - \frac{4\psi_1\psi_2}{(\psi_1 + \psi_2)^2} \sin^2\left(\frac{kL}{2}\right)} \right],$$

giving the acoustic (+) and optical (-) branches.

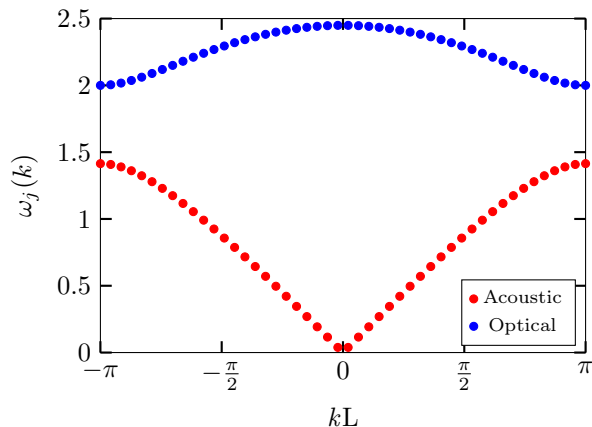


Figure S2: Dispersion relation of the diatomic lattice in the first Brillouin zone ( $-\pi \leq kL \leq \pi$ ). The lower curve (red) is the acoustic branch, which tends to zero frequency at  $k = 0$ , while the upper curve (blue) is the optical branch, which starts at finite frequency. A band gap exists between the two branches when  $\psi_1 \neq \psi_2$ , reflecting the difference in stiffness.

**Acoustic branch (+):** At small wavenumber  $k$ , the frequency tends to zero ( $\omega \rightarrow 0$ ). This corresponds to long-wavelength oscillations where all masses move in phase, similar to a uniform translation. The branch increases approximately linearly with  $k$  near the origin, mimicking sound waves, which is why it is called the acoustic branch.

**Optical branch (-):** At  $k = 0$ , this branch begins at a finite cutoff frequency

$$\omega = \sqrt{\frac{2(\psi_1 + \psi_2)}{m}}.$$

This corresponds to out-of-phase oscillations between the two sublattice masses. The frequency remains finite even for long wavelengths, which is why it is termed the optical branch.

Figure S2 displays both branches across the first Brillouin zone ( $-\pi \leq kL \leq \pi$ ). The periodicity in reciprocal space is visible, as the dispersion repeats with period  $2\pi$ . The band gap between the acoustic and optical branches is set by the difference in coupling constants  $\psi_1$  and  $\psi_2$ . If  $\psi_1 = \psi_2$ , the square-root factor becomes unity and the gap closes, producing continuous bands that meet at the Brillouin zone boundary. For unequal stiffness, a finite frequency gap opens, which is evident in Fig. S2. In this specific plot, the dispersion was computed for a lattice of 48 unit cells, discretizing the Brillouin zone into 48 allowed  $k$ -points. The acoustic branch appears in the lower half, while the optical branch appears in the upper half, with both symmetric about  $k = 0$ .

### S.1.2 Correlation of the Amplitudes

Taking the complex conjugate amplitudes of Eq. (s1), we get,

$$\begin{pmatrix} \gamma & -\tau \\ -\tau^* & \gamma \end{pmatrix} \begin{pmatrix} A_1^* \\ A_2^* \end{pmatrix} = \begin{pmatrix} 0 \\ 0 \end{pmatrix} \Rightarrow \begin{pmatrix} \gamma A_1^* - \tau A_2^* \\ -\tau^* A_1^* + \gamma A_2^* \end{pmatrix} = \begin{pmatrix} 0 \\ 0 \end{pmatrix} \Rightarrow \begin{pmatrix} -\tau A_2^* + \gamma A_1^* \\ \gamma A_2^* - \tau^* A_1^* \end{pmatrix} = \begin{pmatrix} 0 \\ 0 \end{pmatrix} \quad (\text{s2})$$

**Acoustic Branch:** Comparing Eq. (s1) and (s2) gives us the correlation of the amplitudes as

$$A_1 = A_2^* \quad A_2 = A_1^*$$

From Eq. (s1), we can write the equation as,

$$\begin{aligned} \begin{pmatrix} \gamma & -\tau^* \\ -\tau & \gamma \end{pmatrix} \begin{pmatrix} A_1 \\ A_2 \end{pmatrix} &= \begin{pmatrix} 0 \\ 0 \end{pmatrix} \\ \gamma A_1 - \tau^* A_2 &= 0 \\ \Rightarrow \gamma A_1 = \tau^* A_2 &\Rightarrow (\gamma A_1)^2 = (\tau^* A_2)^2 \\ \Rightarrow \gamma^2 (A_1)^2 = (\tau^*)^2 (A_2)^2 &\Rightarrow (\tau \tau^*) (A_1)^2 = (\tau^* \tau) (A_2)^2 \\ \Rightarrow \frac{(A_1)^2}{(A_2)^2} = \frac{\tau^*}{\tau} &\Rightarrow \frac{A_1}{A_2} = \pm \frac{\sqrt{\tau^*}}{\sqrt{\tau}} \end{aligned}$$

Hence,

$$\begin{pmatrix} A_1 \\ A_2 \end{pmatrix} \propto \begin{pmatrix} \sqrt{\tau^*} \\ \pm \sqrt{\tau} \end{pmatrix}$$

**Optical branch:** The nontrivial condition is  $\det = 0 \Rightarrow \gamma^2 - |\tau|^2 = 0$ , so  $\gamma = \pm|\tau|$ . At  $k = 0$  the *optical* mode is out of phase; this corresponds to

$$\gamma = -|\tau|$$

From the first row of Eq. (s1),

$$\gamma A_1 = \tau^* A_2 \Rightarrow \frac{A_2}{A_1} = \frac{\gamma}{\tau^*} = -\frac{|\tau|}{\tau^*} = -e^{i\theta}, \quad \theta \equiv \arg \tau$$

Hence an eigenvector for the optical branch is

$$\begin{pmatrix} A_1 \\ A_2 \end{pmatrix} \propto \begin{pmatrix} 1 \\ -e^{i\theta} \end{pmatrix} = e^{-i\theta/2} \begin{pmatrix} e^{-i\theta/2} \\ -e^{+i\theta/2} \end{pmatrix}.$$

Choose a consistent branch of the complex square root so that

$$\sqrt{\tau} = \sqrt{|\tau|} e^{i\theta/2}, \quad \sqrt{\tau^*} = \sqrt{|\tau|} e^{-i\theta/2}.$$

since  $\sqrt{\tau^*} := -\sqrt{\tau} = e^{-i\theta/2} := -e^{+i\theta/2}$ :

$$\begin{pmatrix} A_1 \\ A_2 \end{pmatrix} \propto \begin{pmatrix} \sqrt{e^{-i\pi} \tau} \\ \pm \sqrt{e^{+i\pi} \tau^*} \end{pmatrix}.$$

## S.2 Spectral Analysis

Normal modes describe synchronous oscillations in which all parts of the system move sinusoidally at a common frequency with fixed phase relations. An elastic system, consisting of masses coupled by harmonic springs, possesses characteristic resonance frequencies. When initial displacements and velocities are applied, the system first exhibits transient dynamics before settling into a steady state over time.

We define the displacement from equilibrium as a time-dependent function across  $N_c$  unit cells, each containing  $N_m$  masses. For a given wave number  $k$ , the system can support multiple frequencies, denoted  $\omega_j(k)$ , where the index  $j$  labels the bands in ascending order, with  $j = 1$  corresponding to the lowest frequency. The complex amplitude of oscillation of the  $n$ -th mass on the  $j$ -th band,  $A_{n,j}(k)$ , is obtained by projecting the displacement  $u_{n,N_i}(t)$  onto that band.

$$A_n(k, \omega_j(k)) = \frac{1}{N_c} \sum_{N_i=1}^{N_c} \frac{1}{\tau_0} \int_0^{\tau_0} u_{n,N_i}(t) e^{ikLN_i} e^{-i\omega_j(k)t} dt \quad (\text{s3})$$

$L$  is the length of the sample and  $\tau_0$  is the time over the sample of elastic waves. Also, the phase of the complex amplitude.

$$\phi_{n,j}(k) = \text{angle}(A_{n,j}(k)) \quad (\text{s4})$$

The dispersion relation is computed by molecular dynamics (MD) simulation with initial conditions  $u_{n,N_i}(0) = \cos(kN_iL)$  and  $\dot{u}_{n,N_i}(0) = 0$ , together with periodic boundary conditions  $e^{ikLN_c} = 1$ , which imply the discrete grid  $kL = 2\pi m/N_c$  (spacing  $\Delta(kL) = 2\pi/N_c$ ). In the second Brillouin zone, we take  $kL \in [-2\pi, 2\pi]$ . Taking into account all springs and integrating the equations of motion using a Runge–Kutta scheme, we obtain the trajectories  $u_{n,N_i}(t)$ . The frequency spectrum is then computed via the finite-time Fourier transform from which the peak locations produce the band frequencies  $\omega_j(k)$ .

$$\ddot{u}_{n,N_i}(\omega) = \frac{1}{\tau_0} \int_0^{\tau_0} u_{n,N_i}(t) e^{-i\omega t} dt \quad (\text{s5})$$

Within the second Brillouin zone, the elastic band structure is generated for all values of the wave number  $k$ . Using the Fourier transform, the frequency of the band structure is calculated at the peak position at a given  $k$ , giving  $\omega_j(k)$ .

In the second set of MD simulations, the band structure is used to prescribe the initial conditions. We take  $u_{n,N_i}(0) = \cos(kN_iL)$  and  $\dot{u}_{n,N_i}(0) = -\omega_j(k) \sin(kN_iL)$ . This sets the velocity consistent with the computed band structure. Each MD simulation yields the displacement  $u_{n,N_i}(t)$ , which is then used to compute the complex amplitude  $A_{n,j}(k)$  of the mass  $n$ -th and its phase  $\phi_{n,j}(k)$ .

### S.3 Berry Vector and Berry Phase

Berry vector for a finite number of unit cells  $N_c$ , can be characterized by,

$$B_V(k) = \sum_{n=1}^{N_m} \tilde{A}_{n,j}^*(k) \tilde{A}_{n,j}(k + \Delta k) \equiv \hat{\alpha}^*(k) \hat{\alpha}(k + \Delta k) + \hat{\beta}^*(k) \hat{\beta}(k + \Delta k) + \dots \quad (\text{s6})$$

Where  $\Delta kL = 2\pi/N_c$ , and  $\tilde{A}_{n,j}(k)$  is the normalized complex amplitude of the unit cell mass  $n$ -th in band  $j$ . This amplitude vector creates a variation of the Berry connection along some path in the complex space as  $k$  varies. For possible  $k$  values of some specific band in the closed path, summing the Berry connection defined by the second Brillouin zone gives the Berry or Zak phase. And each band Berry phases are defined by

$$\chi = -Im \left[ \ln \left( \prod_{i=1}^{N_c-1} B_v(k_i) \right) \right] \text{mod}(2\pi) \quad (\text{s7})$$

The system is discretized at a finite length and  $k$ . In the case of an infinite length of continuous  $k$ , a differential form of the expression is used. The Berry phase is the sum of the unit vector amplitude over the entire manifold for a closed path. The evolution of the unit vector of amplitude in the  $N_m$  dimensional space parametrized by the wave number  $k$  generates a multiplicity.

The Berry phase is dependent on the existence of the closed path in the  $k$ -space along with the amplitude  $\tilde{A}_{n,j}$  being periodic in reciprocal space, which can be affected by the ansatz required to define the system dynamics.

### S.4 Spectrum Analysis & Molecular Dynamics Simulation

For a numerical solution, the initial conditions are set as displacement  $u_{n,N_i}(0) = \cos(kN_iL)$  and velocity  $\dot{u}_{n,N_i} = 0$  for the case of masses. In the first molecular dynamics simulation using the prescribed initial conditions, the dispersion relation is calculated using the temporal integral of the displacement  $u_{n,N_i}(t)$  and the band structure  $\omega_j(k)$  is measured at the span of the wave number  $k$ . The wave number  $k$  has a linear range in  $[-\pi, \pi]$  with an increase of  $2\pi/N_c$  in Brillouin zone 1.

The second set of molecular dynamics simulations has a different initial condition as we have developed the band structure for the system. Using the initial condition as  $u_{n,N_i}(0) = \cos(kN_iL)$  and  $\dot{u}_{n,N_i}(0) = -\omega_j(k) \sin(kN_iL)$ , the displacement of the traveling wave is obtained through the 2nd MD simulation necessary for the solution of the modulus. This initial condition sets the velocity value to the one prescribed by the band structure. One must use a specified traveling elastic wave initial condition to obtain the wave function band structure and the amplitude and phase of the masses. After the second set of MD simulations, we use the displacement  $u_{n,N_i}(t)$  to calculate the complex amplitude, and the phase of the  $n$ th mass and the letter use those to calculate the modulus and the modulus's phase to calculate the system state. Geometrical representation by the Bloch sphere is demonstrated for the superposition of the state (Fig. S3).

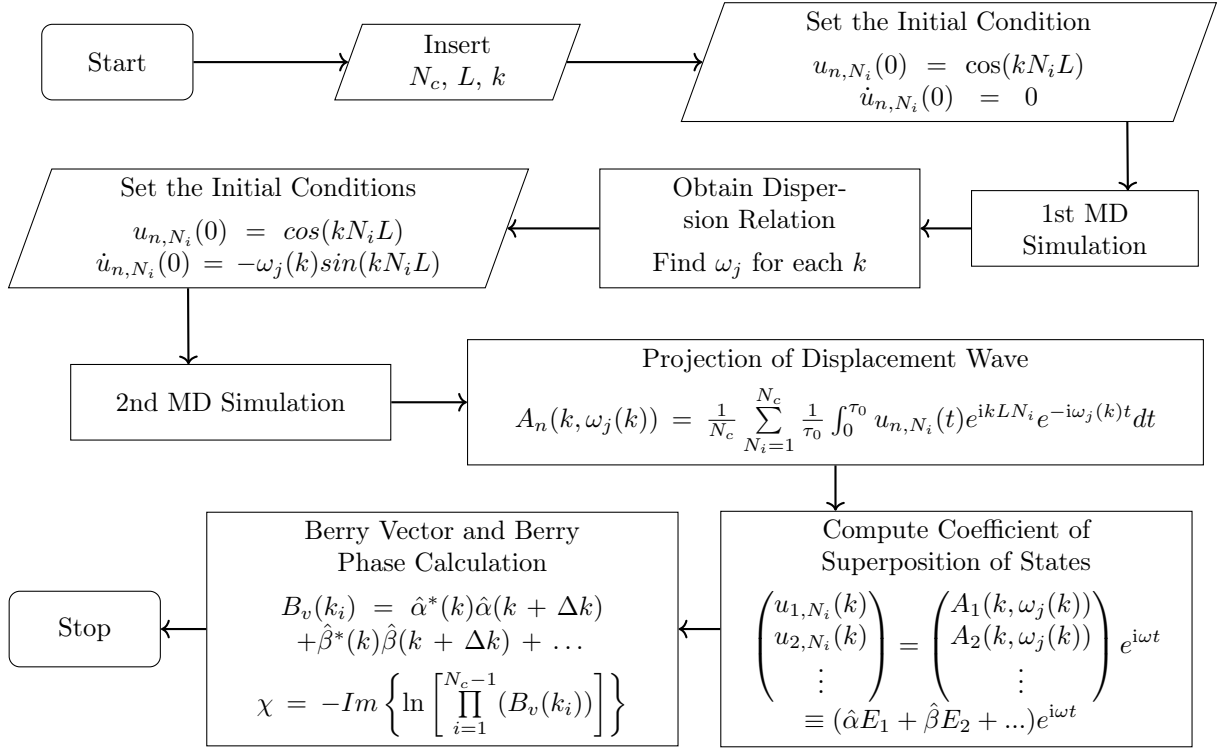


Figure S3: Algorithm for 2-Step Molecular Dynamics (MD) simulation and calculations of coefficients of the superposition of states.